ACS APPLIED MATERIALS & INTERFACES

www.acsami.org

Research Article

Porous Silicon Carrier Endowed with Photothermal and Therapeutic Effects for Synergistic Wound Disinfection

Wei Duan, Xingyue Liu, Jingwen Zhao, Yongke Zheng,* and Jianmin Wu*

Cite This: *ACS Appl. Mater. Interfaces* 2022, 14, 48368−48383

Read Online

ACCESS | Metrics & More | Article Recommendations | Supporting Information

ABSTRACT: Drug carriers endowed with photothermal effects will allow the drug delivery system to release drugs in a thermal-stimuli manner. In addition, the photothermal therapy (PTT) will also interplay with therapeutic drugs loaded in the carrier to exhibit synergistic bioactivity for various disease treatment. However, endowing the drug carrier with photothermal and synergistic therapeutic effects still has challenge. Herein, we demonstrate that surface modification of porous silicon (PSi) with polydopamine (PDA) could endow the classical drug carrier with a significant photothermal effect for advanced antibacterial therapy and wound disinfection. Specifically, the PSi surface interacts with a Cu^{2+}/PDA complex via a simple and fast surface reduction-induced deposition method, forming the unique CuPDA coated PSi microcarrier (CuPPSi) without blocking the mesoporous structure. The CuPPSi carrier generates a higher near-infrared (NIR) photothermal efficiency and improved drug loading capacity owing to the abundant functional groups of PDA. Stimuli-responsive release of antibacterial Cu^{2+} and loaded curcumin (Cur) from CuPPSi can be realized under multiple stimuli including pH, reactive oxygen species and NIR laser irradition. Benefited from the carrier's intrinsic multimodal therapy, the CuPPSi-Cur platform exhibits amplified, broad-spectrum, and synergistic antibacterial effect, killing more than 98% for both *Staphylococcus aureus* and *Escherichia coli* at a mild PTT temperature (~45 °C). Notably, the combined therapy promotes migration of fibroblasts with no significant cytotoxicity as revealed through cell experiments *in vitro*. In bacteria-infected mice model, efficient bacterial ablation and wound healing are further demonstrated with negligible side effects *in vivo*. Overall, the rational design of a drug carrier with photothermal and therapeutic effects provides a novel intervention for amplifing wound disinfection clinically.

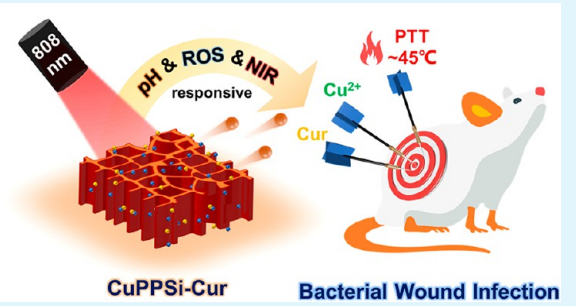

KEYWORDS: *wound disinfection, functional drug carrier, mild-temperature photothermal therapy, stimuli-responsive drug release, porous silicon*

1. INTRODUCTION

Infectious diseases induced by pathogens such as viruses, bacteria, and fungi have become a prominent threat to human health.[1,2] Over the past few decades, antibiotics have been inevitably and extensively utilized in clinical practice to treat a bacterial infection, saving millions of lives.[3] However, the misuse and abuse of antibiotics have led to the multiple drug resistance of bacteria, large-scale environmental pollution, and severe toxic side effects.[4] Therefore, much effort has been devoted to develop safe, efficient, and antibiotic-free therapeutic strategies for easing the burden to the environment and society. Up to now, various new bactericides including antimicrobial peptides, natural herbs, quaternary ammonium compounds, metal ions, and metal nanomaterials (Ag and Cu) have been developed as alternative antibacterial agents.[5−11] On the other hand, a large number of research work has focused on the efficient antibacterial drug delivery systems (DDS) to enhance drug bioavailability and minimize side effects.[12] Nevertheless, dosage control of therapeutic agents still faces challenges in traditional DDS. Drug delivery capable of stimuli-responsive release of antibacterial agents requires smart functional carriers that can control local drug dosing. With this DDS platform, the loaded drug can be released in a manipulated or programmable manner, so that the dose of a therauptic drug can be varied with the disease progress or healing. In the past decade, several drug carriers such as polymers, nanomaterials, and liposomes have been functionalized for developing smart DDS that could respond to various types of intrinsic stimuli at the infection site, enabling remarkable efficacy in antibacterial therapy.[13]

Skin wounds infected by bacteria usually cause pain and inflammation, which reduces the quality of wound healing and may even lead to amputation.[14,15] For the development of on-

Received: July 6, 2022
Accepted: October 13, 2022
Published: October 24, 2022

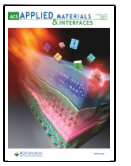

https://doi.org/10.1021/acsami.2c12012
ACS Appl. Mater. Interfaces 2022, 14, 48368−48383

Scheme 1. Schematic Illustration for the Preparation of PSi Carrier Endowed with PTT Effect as a Multi-Stimuli-Response DDS Platform for Synergistic Wound Disinfection

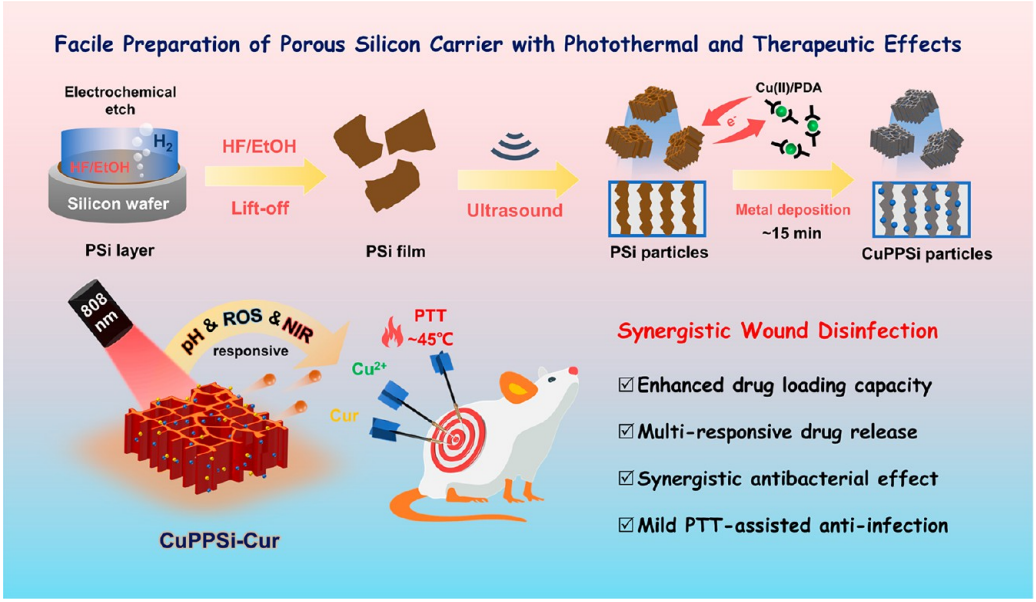

demand DDS targeted at bacteria-infected wound, internal stimuli such as pH and reactive oxygen species (ROS) are effective because the increased metabolic activation upon infection leads to the acidic and high oxidative stress in wound inflammatory environments.[16,17] In addition to the intrinsic stimuli by wound sites, many types of external stimuli including mechanical strain, ultrasound, electric field, magnetic field, and light to remotely trigger the release of therapeutic payloads have been investigated.[18,19] Notably, the use of a near-infrared (NIR) laser in light-triggered DDS has exhibited several advantages in clinical applications owing to good tissue penetration, remote controllability, and site specificity.[20] Besides, bacteria are heat-sensitive, and high temperature treatment can lead to significant bacterial inactivation.[21] Photothermal therapy (PTT) using NIR laser irradiation has provided an efficient alternative for local bacterial killing, which has received broad attention in recent years. Hence, it is reasonable to expect that a drug carrier itself endowed with a photothermal effect would not only control the loaded drug release in a thermal-stimuli manner under NIR laser irradiation but also enhance the antibacterial efficiency by the interplay with therapeuic drug loaded in the carrier. Development of a drug carrier with intrinsic PTT and a capability of stimuli-responsive drug release might be an important avenue to boost bacterial elimination efficiency. The synergy between the thermal effect and the drug payload could also reduce the overheating damage on the healthy host cells or tissues caused by the temperature (~70 °C) required for PTT alone.[22,23] However, conventional photothermal agents such as organic molecules, 2D nanomaterials, noble metal nanoparticles, and metal sulfide/oxide nanomaterials have limited drug loading capacity, unsatisfied biocompatibility, insufficient biodegradation, and uncontrollable release of drugs. There is still an urgent need to exploit drug carrier materials with photothermal and therapeutic effects for efficient and controllable DDS.

Porous silicon (PSi) has a large surface area, abundant pore structures, adjustable surface chemistry, good biocompatibility, drug protective abilities, and oxidative-stimuli responsive release properties, which make it attractive as a therapeutic drug vehicle for the development of advanced DDS.[24−27] A further evolution for the construction of high-performance DDS is to endow the drug carrier itself with a therapeutic function such that it no longer serves as a mere passive vehicle to deliver drugs at the target tissue but itself can be regarded as a therapeutic agent.[28] The codelivery of therapeutic drugs and carriers with a bioactive function is expected to achieve an enhanced or a synergistic therapeutic effect higher than using drugs alone. Our previous work demonstrated that PSi is a good biodegradable drug delivery carrier with therapeutic functions owing to the released inorganic Si ions upon degradation at physiological conditions.[29] After loaded with vascular endothelial growth factor (VEGF), the codelivery system could release Si ions and VEGF as the Si skeleton dissolved, thereby realizing efficient and synergistic angiogenesis therapy in tissue or wound repair. Further, we can speculate that release of bioactive ions could be manupilated by thermal stimuli owing to the temperature-dependent biodegradation kinetics of the PSi carrier. However, the PSi material itself lacks a NIR photothermal characteristic, which restricts the development in photothermal stimuli DDS for multimodal treatment. To address the issue, further design and fabrication of the PSi vehicle endowed with a photothermal effect for enhanced drug delivery and synergistic therapy holds significant incentives for clinical wound disinfection.

Inspired by the facts above, we propose a new strategy to endow the classical PSi carrier with significant photothermal and therapeutic effects for synergistic antibacterial therapy. By *in situ* reduction of a Cu^{2+}/polydopamine (PDA) mixture on fresh-etched PSi particles, CuPDA coated PSi (CuPPSi) was successfully prepared via a simple and fast surface reduction-induced deposition method in acidic aqueous solutions. The modification process is highly compatible for the PSi material, and a homogeneous surface coating was formed without blocking the mesoporous structure. With the assitance of external NIR photothermal stimili and wound site environmental changes such as pH and ROS, codelivery of antibacterial ion/drug for synergistic bacteria killing and wound disinfection could be achieved (Scheme 1). Accord-

https://doi.org/10.1021/acsami.2c12012
ACS Appl. Mater. Interfaces 2022, 14, 48368−48383

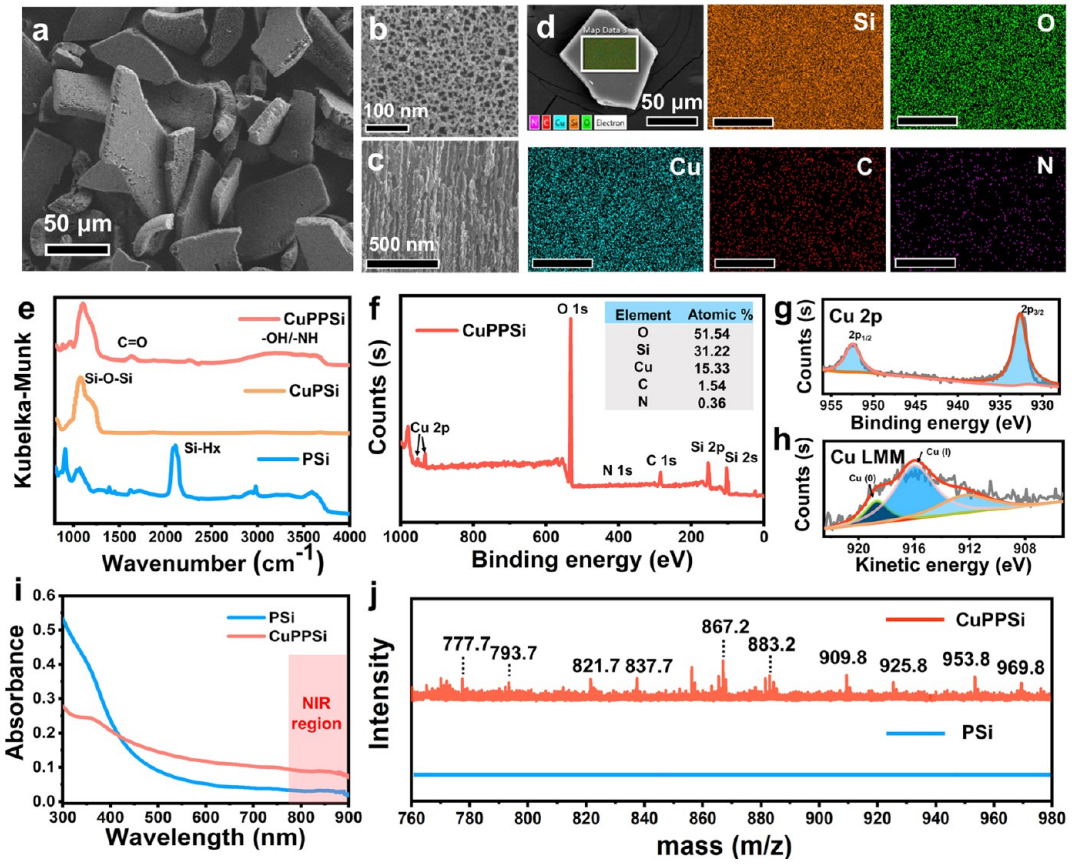

Figure 1. Synthesis and characterization of CuPPSi particles. (a) Representative SEM image of CuPPSi particles. SEM images of CuPPSi particles from top-view (b) and cross section view (c). (d) Elemental mappings of Si, O, Cu, C, and N signals in CuPPSi. The unmarked scale bars in panel d are 20 μm. (e) DR-FTIR analysis of the PSi, CuPSi, and CuPPSi particles. The XPS full scan spectrum (f), high-resolution Cu 2p XPS spectrum (g), and Cu LMM spectrum (h) for as-synthesized CuPPSi samples. (i) UV−visible absorption spectra of PSi and CuPPSi particles. (j) MALDI-TOF MS spectra of PSi and CuPPSi particles.

ingly, the PSi vehicle coated with a CuPDA layer has several advantages over traditional DDS: (I) PDA has good biocompatibility and excellent photothermal conversion efficiency, thus endowing PSi with NIR photothermal activity and PTT function. (II) Compared to other metallic materials (Ag, Au), Cu has well-known antibacterial properties, and is more cost-effective and easy to produce.[30] The bactericidal Cu ions released from CuPPSi carrier can have broad antibacterial efficacy for wound disinfection. (III) As a common melanin-like biopolymer, PDA has abundant functional groups including catechols, amine, and aromatic rings, which enables a higher payload and controlled release of therapeutic molecules via hydrogen bonding or $\pi-\pi$ stacking.[31] In the present work, curcumin (Cur) was chosen as a bioactive natural molecule to be loaded in the CuPPSi carrier because of its antioxidant, antibacterial, and anti-inflammatory activities. However, the major limiting factor of Cur is its lipophilic nature and low stability in biological conditions, that reduces its bioavailability.[32,33] After loading in CuPPSi, self-degradation of Cur antioxidant bioactivity could be greatly inhibited ascribing to the protective effect of the microcarrier, thereby better exerting their biological activities. A two-component therapeutic approach comprising antibacterial Cur and Cu ions resulted in a synergistic effect for bacteria killing. Under the internal stimulation of pH and ROS or the external NIR irradiation, on-demand release of Cu^{2+} and Cur from Cur-loaded CuPPSi (CuPPSi-Cur) was observed because these factors significantly affected the desorption of Cur as well as the release of Cu^{2+} from CuPPSi, thereby achieving the high-performance bacteria killing effects. Furthermore, the antibacterial activity of CuPPSi-Cur could be significantly augmented when combined with PTT at a mild temperature (~45 °C). Both *in vitro* and *in vivo* results further demonstrated that the developed mild-temperature PTT nanoplatform was highly compatible to normal skin cells and tissues without overheating damage in traditional PTT, displaying the strongest antibacterial and anti-infective properties under rational NIR power. This PSi carrier with photothermal and therapeutic effects provided a promising synergistic platform to combat the growth of bacteria for wound healing and other infective diseases in a safe, mild, and efficient way.

2. RESULTS AND DISCUSSION

2.1. Preparation and Characterization of CuPPSi Microcarrier. PSi microparticles were synthesized according to a previously reported method (Scheme 1).[34,35] Briefly, the PSi layer was first prepared by electrochemical etching of a silicon wafer (p++ type) in hydrofluoric acid/ethanol (HF/EtOH, V/V = 4:1) solutions. As measured by the spectroscopic liquid infiltration method (SLIM), the porosity and thickness of the PSi layer were ~60% and 20 μm, respectively. After electrochemical etching and SLIM measurments, the PSi layer was lifted off the Si wafer by a current-

https://doi.org/10.1021/acsami.2c12012
ACS Appl. Mater. Interfaces 2022, 14, 48368−48383

assisted approach to obtain the PSi film. Then, the free-standing PSi film was broken down through ultrasonication to prepare PSi microparticles. A scanning electron microscopy (SEM) image indicated the porous structure of PSi particles. As shown, PSi displayed a microscale size of ~100 μm with a pore diameter of ~20 nm (Figure S1a,b). The cross-sectional SEM images revealed that the vertical pore channels crossed over the PSi particles (Figure S1c).

Driven by the desire for endowing the PSi with PTT function, a novel "one stone, three birds" strategy was proposed for surface modification of PSi particles, which could impart the porous microcarrier with PTT function, antibacterial property, as well as versatile surface groups. To achieve facile and convenient modification, dopamine was chosen because it is a mussel-inspired molecule that belongs to the catecholamines class and tends to interact with a variety of substrates strongly via both covalent or noncovalent binding.[36] In addition, its polymerization product, PDA, is able to form and stably bind on almost all material surfaces, including metals, synthetic polymers, ceramics, and semiconductors.[37] Owing to the simple preparation process, excellent biosafety, strong adhesive property, and high photothermal conversion ability, PDA-based modification has been extensively explored as a versatile strategy to functionalize drug carrier surfaces.[38] However, self-polymerization of DA only occurs under alkaline solutions using oxygen as the oxidant, and the process usually takes a few hours to days.[39] The method is not suitable for coating PDA layer on PSi surface, since the long-time exposure to alkaline solution will dissolve the PSi. Interestingly, it has been found that using Cu^{2+} rather than O_2 as the oxidant can significantly accelerated the polymerization of DA even at acidic solution,[40] which is compatible to PSi frameworks. However, homogeneous surface coating of PDA on mesoporous materials without blocking its pore structure is still a challenge. Previous investigation shows that PDA prepared by Cu^{2+} catalyzed polymerization exists in the form of a Cu^{2+}/PDA complex.[40,41] In the present study, we proposed a reduction-induced surface coating approach, in which a PSi skeleton simultaneously acted as a template and reducing agent since the freshly etched PSi contained abundant Si−H terminals (Scheme 1).[42] In the surface reduction process, Cu^{2+} in the Cu^{2+}/PDA complex was able to withdraw electrons from the surface hydrides (Si−H_x) of the PSi skeleton. The *in situ* reduction of Cu^{2+} in the Cu^{2+}/PDA complex could tightly attach PDA on the surface of PSi, forming a homogeneous PDA layer within several minutes. In addition, the coordination of Cu^{2+} with PDA decreased its reduction potential, making the galvanic displacement milder and facilitating the formation of thinner polymer layer without blocking the mesoporous structure for drug delivery application.

The morphology of the as-prepared CuPPSi particles was characterized by SEM. As shown in Figure 1a, the macroscopic appearance of CuPPSi maintained a similar size and morphology compared to PSi (Figure S1). The high-magnified SEM images of CuPPSi samples from both top and cross-sectional views showed the PDA decorated-PSi particles retained a highly mesoporous structure (Figure 1b,c). The presence of CuPDA coating on CuPPSi was confirmed by energy-dispersive X-ray spectroscopy (EDS). The elemental mapping images (Figure 1d) clearly showed the presence of Si, O, Cu, C, and N elements in a representative CuPPSi particle, which could also be observed in the corresponding EDS elemental mapping of the cross-sectional SEM image (Figure S2). To further validate the presence of the chemical group of PDA on CuPPSi, different samples including PSi, Cu-decorated PSi (CuPSi), and CuPPSi were characterized using diffuse reflection-infrared Fourier transform infrared (DR-FTIR) spectroscopy. As demonstrated in Figure 1e, rich Si−H_x bonds at 2100 cm^{-1} were observed in DR-FTIR spectra for the freshly prepared PSi particles, while the Si−H_x bonds were consumed and disappeared in the CuPSi particles. At the same time, the peak at 1056 cm^{-1} (Si−O−Si stretching vibration) was clearly observed in CuPSi samples, further confirming the oxidation of PSi during the Cu deposition. Compared to CuPSi, the DR-FTIR spectra of CuPPSi particles showed a broad absorptive band in the range of 3100−3650 cm^{-1}, which was due to the stretching vibrations of O−H and/or N−H in the PDA chains. In addition, the absorption bands in the range of 1625−1650 cm^{-1} corresponded to the bend vibrations of C=O and/or O−H stretching from catechol groups in the PDA polymeric chains.

Then, X-ray photoelectron spectrometry (XPS) characterizations were performed to further gain insights into the electron states and the surface chemical composition of elements in CuPPSi. The full survey spectra of XPS revealed that the CuPPSi sample contains Si, Cu, O, C, and N elements (Figure 1f), which were consistent with the elemental mapping results in the SEM measurement. The high-resolution spectra of Cu 2p showed two strong peaks located at 932.7 and 952.3 eV, which corresponded to the electron states of Cu $2p_{3/2}$ and Cu $2p_{1/2}$ peaks, respectively (Figure 1g) .[43] It should be noted that the satellite peak of Cu(II) was not observed in the position of main peaks in the CuPPSi samples, indicating the complete reaction between Cu(II) and PSi in the formation of CuPPSi. The Si−O−Cu bond was observed from the high-resolution Si 2p spectrum of CuPPSi, further validating the occurrence of the deposition reaction (Figure S3a). However, it is difficult to distinguish Cu(I) and metallic Cu(0) from the Cu 2p XPS spectra because they have similar binding energies. Therefore, X-ray excited auger electron spectroscopy (XAES) was utilized to study the compositions of the Cu(I) and Cu(0) species in CuPPSi. As indicated in the Cu LMM XAES spectra (Figure 1h), two peaks appeared at 916 and 918.7 eV were corresponding to Cu(I), and Cu(0) species, respectively.[44] The shoulder peak located at 912 eV was assigned to an extra Gaussian−Lorentzian band to eliminate the effect of other orbital electrons on the XAES.[45] The presence of Cu(I) in CuPPSi might be attributed to the coordination bonding formation between Cu and PDA or the subsequent mild oxidation of Cu(0) in the air. The high-resolution N 1s and C 1s spectra further verified the coordination interaction (Cu−N, Cu−C) between Cu and PDA (Figure S3b,c). The copper and cuprous are easily oxidized and the sustainably released Cu ions is expected to play the antibacterial role for future biomedical applications.[46] Based on the above results, the reaction between PSi and Cu(II) can be expressed as the following equations.

Oxidation:

$$\mathrm{Si} - \mathrm{H}_x + 2\mathrm{H}_2\mathrm{O} \rightarrow \mathrm{SiO}_2 + (4 + x)\mathrm{H}^+ + (4 + x)\mathrm{e}^- \quad (1)$$

Reduction:

$$\mathrm{Cu(II)} + \mathrm{e}^- \rightarrow \mathrm{Cu(0)/Cu(I)} \quad (2)$$

https://doi.org/10.1021/acsami.2c12012
ACS Appl. Mater. Interfaces 2022, 14, 48368−48383

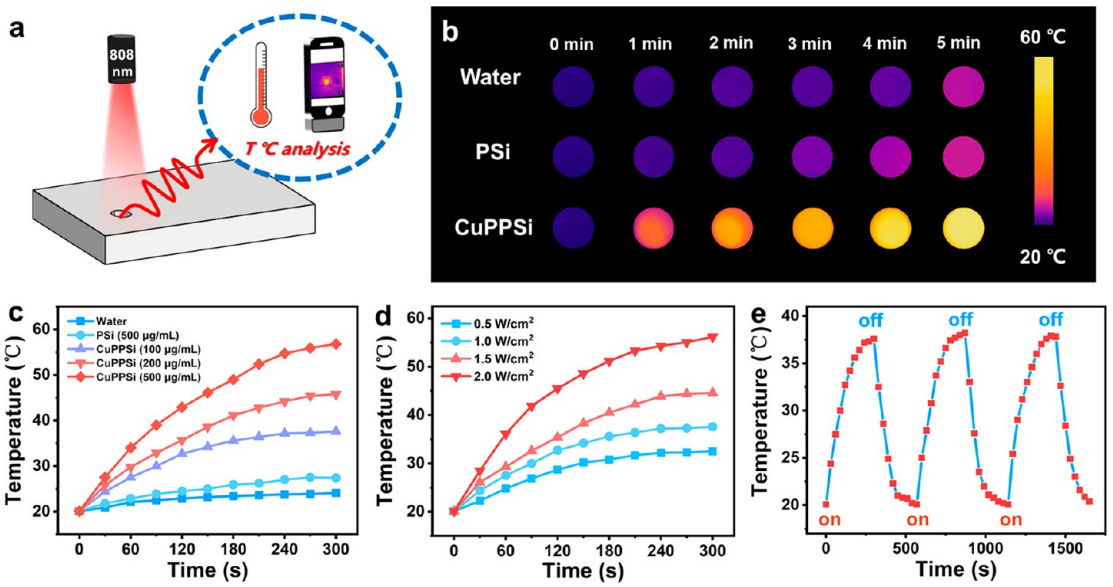

Figure 2. (a) Schematic illustration for the setup to test photothermal property. (b) Thermal images of different samples in 5 min including water, PSi particles (500 μg/mL), and CuPPSi particles (500 μg/mL) under the NIR laser irradiation (1.0 W/cm^2). (c) Photothermal curves of water, PSi particles (500 μg/mL), and CuPPSi particles (100, 200, 500 μg/mL) under the NIR laser irradiation (1.0 W/cm^2). (d) Comparison of the photothermal effects of CuPPSi particles (100 μg/mL) under the NIR laser irradiation with different power densities. (e) Temperature elevation curves of CuPPSi particles (100 μg/mL) over three rounds of on/off cycling under the NIR laser irradiation (1.0 W/cm^2).

The higher NIR absorption is the prerequisite to improve the photothermal conversion efficiency. To confirm the NIR absorption ability, UV−vis-NIR spectroscopy of PSi and CuPPSi was measured. As demonstrated in Figure 1i, CuPPSi presented a stronger absorption than the equivalent concentration of bare PSi from 780 to 900 nm in the NIR region, owing to the NIR absorbance of the decorated PDA on the CuPPSi. Furthermore, matrix-assisted laser/desorption ionization time-of-flight mass spectrometry (MALDI-TOF MS) was also conducted to investigate the surface chemistry of CuPPSi and bare PSi particles. Compared to PSi samples, characteristic cluster peaks in CuPPSi appeared and the m/z value difference between adjacent cluster peaks is ∼16 Da (Figure 1j), which was assigned to OH leaving. The phenomenon is often observed in the identification of melanin with mass spectrometry.[47] Overall, the successful preparation of CuPPSi particles and the mechanism of surface reaction were verified by the results of material characterization.

2.2. Photothermal Effect of CuPPSi Microcarrier. PDA has been regarded as a promising NIR photothermal agent with good biocompatibility.[37,39] The modification of PDA on PSi also imparts good NIR photothermal conversion efficiency to CuPPSi particles. Figure 2a illustrates the smartphone compatible device for photothermal measurement. Under the laser irradiation at 808 nm, the photothermal materials can efficiently transfer the light energy to heat energy, resulting in the sharp increase of temperature, which can be easily recorded and photographed by a hand-held thermal imager attached to a mobile phone. For comparison, the photothermal effects of PSi and CuPPSi particles with various concentrations were tested under 808 nm NIR laser irradiation. As shown in the infrared thermal imaging pictures (Figure 2b), a rapid temperature rise in the CuPPSi group was observed after 808 nm laser irradiation for 5 min. The extent of temperature rising increased accordingly with the increase of CuPPSi concentration (Figure 2c). For comparison, the temperature of 500 μg/mL CuPPSi increased to 56 °C, while it only increased to 25 °C with the same concentration of PSi. The temperature increases of the CuPPSi particles presented an irradiation density-dependent manner (Figure 2d). Additionally, the as-prepared CuPPSi exhibited reversible photothermal activity without significant variation in the maximum PTT temperature after 3 cycles of a heating and cooling process (Figure 2e). The excellent photothermal effect of the CuPPSi carrier greatly expands the possibilities to develop efficient DDS endowed with PTT effect for versatile biomedical applications.

2.3. Loading and Antioxidant Activity of Cur in CuPPSi. As a plant-derived polyphenolic active substance with low side effects, curcumin (Cur) has been applied clinically for broad-spectrum antibacteria and skin wound healing.[32,48] However, the major problem in the application of Cur alone as a therapeutic agent is the poor aqueous solubility as well as the rapid degradation of Cur at physiological pH, leading to low bioavailability and low efficiency in an aqueous-based therapeutic system.[49] To solve this problem, attempts have been made to load Cur within colloidal nano/microparticles for enhancing its bioavailability.[50] However, most nanocarriers only serve as a mere passive vehicle to deliver drugs and lack the bioactive and therapeutic functions. In the present work, CuPPSi with a mesoporous structure may protect the Cur payload and increase its bioavailability since PSi can isolate the payload from the biodegradation factors and is more hydrophilic than the Cur itself. In addition, CuPPSi with photothermal and therapeutic effects could be expected to construct smart DDS to release a drug in a pH, ROS, and thermal-stimuli manner. Furthermore, CuPPSi-mediated PTT will also interplay with released Cur and Cu ions, thereby exhibiting synergistic bioactivity for antibacterial treatment.

To quantify the drug-loading capacity, free Cur concentrations in the solution before and after loading in PSi and CuPPSi were determined by UV−vis absorption at 425 nm according to a standard curve (Figure S4). The loading capacity of Cur was determined to be 11% and 35% for PSi and CuPPSi, respectively (Figure 3a). The significantly

https://doi.org/10.1021/acsami.2c12012
ACS Appl. Mater. Interfaces 2022, 14, 48368−48383

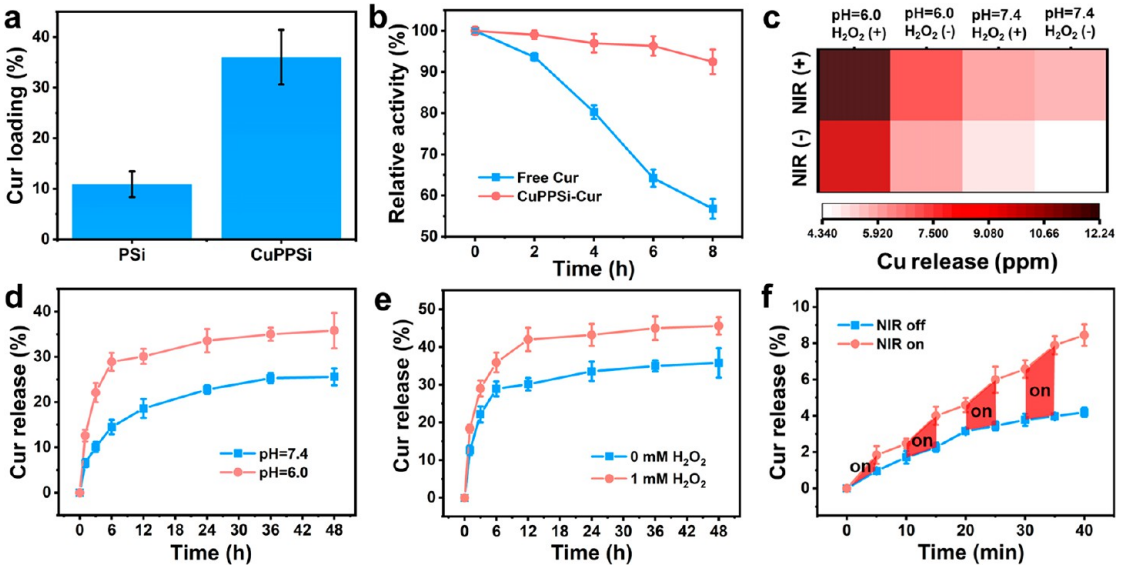

Figure 3. (a) Cur loading efficiency of PSi and CuPPSi carrier. (b) Comparison of the relative antioxidant activity of free Cur and CuPPSi-Cur in PBS (pH = 7.4, 37 °C). (c) Heat map of Cu ion release from CuPPSi-Cur particles incubated in different conditions after 48 h. (d) Release curve of Cur from CuPPSi-Cu particles at different pH values in PBS (0 mM H_2O_2, 37 °C). (e) Cur release curve from CuPPSi-Cur particles with or without the addition of 1 mM H_2O_2 in PBS (pH = 6.0, 37 °C). (f) Release curve of Cur from CuPPSi-Cur particles with or without the NIR laser irradiation (808 nm, 1.0 W/cm^2, 5 min each time). The error bars represent mean ± SD (**$p < 0.01$, $n = 3$).

enhanced drug loading efficiency might be attributed to the interaction between aromatic Cur and PDA on CuPPSi via $\pi-\pi$ stacking, hydrogen bond and hydrophobic interaction.[51] To confirm the presence of Cur in CuPPSi-Cur, DR-FTIR spectra were further measured. We can observe the more obvious O−H bending vibration in the range of 3100−3650 cm^{-1} and C=O/C=C stretching vibrations in the range of 1625−1650 cm^{-1} (Figure S5). These FTIR peaks assigned to the Cur molecules proved the successful preparation of CuPPSi-Cur.

Cur is an excellent antioxidant that can scavenge excess ROS produced in the microenvironment of the infected wound.[52] However, Cur is easily hydrolyzed or degraded in an aqueous solution, leading to the decrease of bioavailability.[49] To elucidate whether the CuPPSi can protect and preserve the Cur, the antioxidant activity of Cur before and after loading in a CuPPSi microcarrier was studied by monitoring the DPPH scavenging efficiency in PBS and cell culture media (pH = 7.4, 37 °C) within 8 h (Figure 3b and Figure S6). As a result, over 90% activity remained in the CuPPSi-Cur sample after incubation in PBS or cell culture media for 8 h. On the contrary, the free Cur dissolved in PBS and cell culture media only retained 55% and 42% of its initial DPPH scavenging efficiency after 8 h, respectively. The results indicate that CuPPSi can significantly protect the antioxidant Cur from inactivation, thereby better exerting its biological activities.

2.4. Stimuli-Responsive Release Behavior of Cu^{2+} and Cur. Drug release in PSi-based DDS could be ascribed to two mechanisms. One is the degradation of the Si skeleton and another is the diffusion of the loaded drug.[53] It has been well-documented that the Si framework of PSi has a good biodegradable ability: the loaded drugs and ions will release as the degradation progresses.[29,54] To confirm this, the amount of Si ion release in the different simulated body fluids was measured by inductively coupled plasma optical emission spectrometry (ICP-OES). As indicated in Figure S7, both ROS and the alkaline environment accelerated the Si skeleton degradation of CuPPSi and the release of Si ions, showing the same phenomenon with our previous work.[53] In addition, the release of Si ions from CuPPSi could be accelerated under the stimulation of NIR at different physiological aqueous conditions owing to the temperature elevation. Meanwhile, the CuPPSi-Cur delivery platform could also sustainably release Cu^{2+}, a well-known antibacterial agent, for bacterial therapy. As characterized in Figure 1g, the precursor of Cu^{2+} in CuPPSi should be in the form of Cu(0)/Cu(I). Therefore, the release of Cu^{2+} needs an oxidation process. The slightly acidic and high ROS level, two characteristics of infected wound environments, could dominate the release of Cu^{2+} from CuPPSi-Cur, since the degradation rate of the PSi skeleton in an acidic environment is relatively slow. To prove this, the release behaviors of Cu^{2+} from CuPPSi in different pH values and ROS (represented by H_2O_2) levels were studied by ICP-OES. As shown, the Cu^{2+} release from the CuPPSi was remarkably accelerated in the presence of high H^+ and H_2O_2 concentrations (Figure 3c). The mechanism could be explained by the following equations.

$$Cu(0) + H_2O_2 + 2H^+ = Cu^{2+} + 2H_2O \quad (3)$$

$$2Cu(I) + H_2O_2 + 2H^+ = 2Cu^{2+} + 2H_2O \quad (4)$$

We found the Cu^{2+} release from the CuPPSi-Cur was markedly enhanced with NIR irradiation. For instance, the release of Cu^{2+} from the CuPPSi-Cur system under NIR irradiation after 48 h of incubation with 1 mM H_2O_2 at pH 6.0 increased 27% compared to that of the group without NIR irradiation. In other experimental groups, similar trends were also observed.

On-demand drug delivery has proved to be a more efficient approach for precise therapy of bacterial infection. Acid or ROS-sensitized vehicles have received much attention owing to the mildly acidic and highly oxidative microenvironment in infected wounds.[55,56] Thus, Cur release profiles of CuPPSi-Cur were evaluated under different pH or ROS conditions. As shown in Figure 3d, the release percentage of Cur was 25.5%

https://doi.org/10.1021/acsami.2c12012
ACS Appl. Mater. Interfaces 2022, 14, 48368−48383

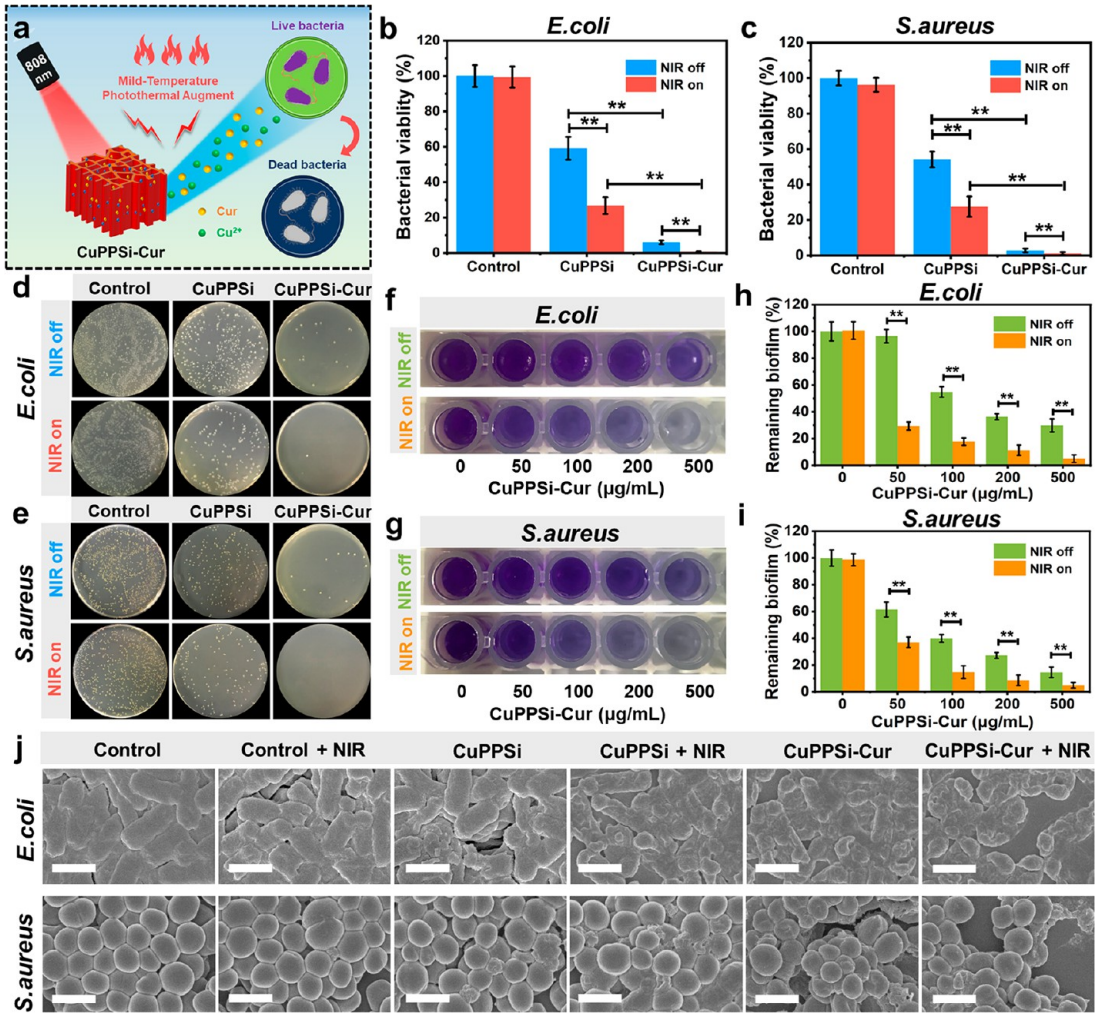

Figure 4. Antibacterial performance evaluation *in vitro*. (a) Schematic illustrates mild-temperature photothermal augmented bacteria killing capability by CuPPSi-Cur platform. Bacterial viability of *E. coli* (b) and *S. aureus* (c) after treated with Control (PBS), CuPPSi (200 μg/mL), CuPPSi-Cur (200 μg/mL) without or with NIR laser irradiation (1.0 W/cm^2, 10 min). Typical photographs of *E. coli* (d) and *S. aureus* (e) colonies after treated with Control (PBS), CuPPSi (200 μg/mL), CuPPSi-Cur (200 μg/mL) without or with NIR laser irradiation (808 nm, 1.0 W/cm^2, 10 min). Typical photographs of *E. coli* (f) and *S. aureus* (g) biofilms by crystal violet staining after treated with different concentrations of CuPPSi-Cur without or with NIR laser irradiation (1.0 W/cm^2, 10 min). Relative remaining biomass of *E. coli* (h) and *S. aureus* biofilms (i) after treated with CuPPSi-Cur without or with NIR laser irradiation (1.0 W/cm^2, 10 min). (j) SEM images of biofilms formed by *E. coli* and *S. aureus* after different treatments. The scale bars are 1 μm. The error bars represent mean ± SD (**p < 0.01, n = 3).

within 48 h at pH 7.4. In contrast, the percentage of Cur release increased 35.8% within 48 h at pH 6.0, which was a common pH in infected tissue. Such an acid-accelerated Cur release behavior was ascribed to the protonation of amine groups, which could result in the disruption of $\pi-\pi$ interactions between Cur and PDA.[31,57] In addition, the release behavior of Cur in the absence or presence of ROS (represented by H_2O_2) was also studied. As shown in Figure 3e, the improved release of Cur was observed when 1 mM H_2O_2 was added in the test solution (pH 6.0). The accumulative Cur release could reach 45.6% after 48 h, which is almost 10% higher than that in the absence of H_2O_2, possibly due to the breakage of hydrogen bonding between Cur and PDA through oxidization of PDA's polyphenol groups as well as the oxidation-induced CuPPSi degradation.[53,57]

Compared with internal pH and ROS stimuli, using NIR as external stimuli for drug delivery control exhibits several advantages such as high tissue penetration, low tissue harm, easy operation, and spatiotemporal precise control of treatment.[58] CuPPSi microcarriers with PTT function could be utilized as NIR-responsive DDS for controlled release of a drug. As indicated in Figure 3f, the Cur releasing rate from CuPPSi-Cur can be controlled by the NIR laser irradiation. After four cycles of "on−off" NIR laser irradiation for 40 min (each cycle including 5 min NIR on and 5 min NIR off), the cumulative Cur release reached ∼8.5%. For comparison, the cumulative Cur release was only ∼4.1% over equal amount of time in the absence of NIR laser irradiation, indicating the PSi carrier with photothermal function could further trigger the Cur release in a thermal-stimuli manner.

2.5. The Antibacterial and Antibiofilm Properties.

PTT has been widely used recently in the biomedical field for bacterial infected wound treatment.[58,59] However, a relatively high temperature (>50 °C) would cause overheating damage on surrounding normal cells and tissues of the wounds in traditional PTT. Encouraged by the novel CuPPSi-Cur therapeutic platform that achieves the synergistic functions of codelivery, on-demand and NIR-responsive release of two

https://doi.org/10.1021/acsami.2c12012
ACS Appl. Mater. Interfaces 2022, 14, 48368−48383

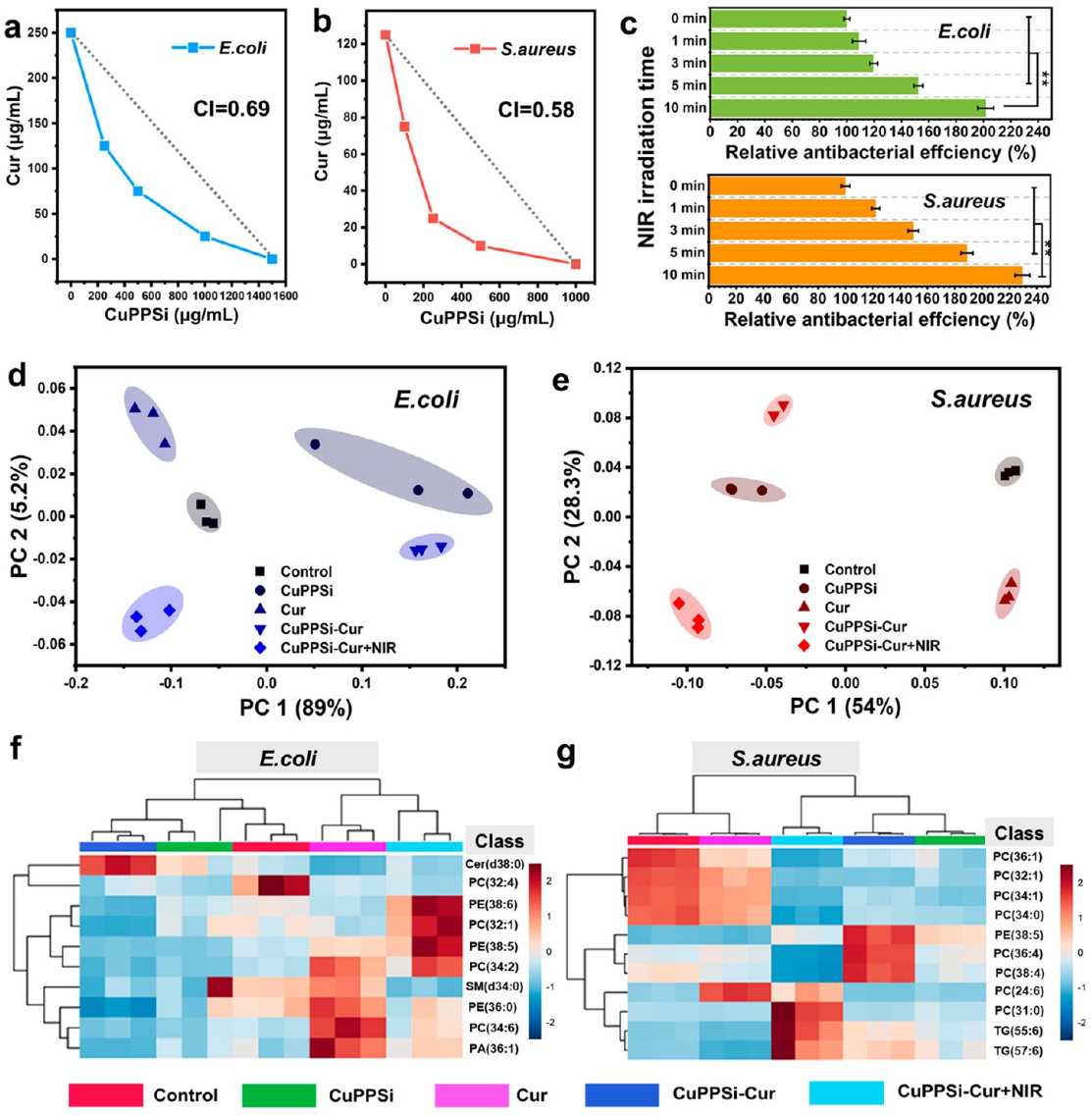

Figure 5. Interaction curve of CuPPSi and Cur for *E. coli* (a) and *S. aureus* (b). (c) The relative antibacterial efficiency of *E. coli* and *S. aureus* after treatments with CuPPSi-Cur (200 μg/mL) under different NIR irradiation times. The error bars represent mean ± SD (**$p < 0.01$, $n = 3$). The principal component analysis (PCA) results of lipid metabolites for *E. coli* (d) and *S. aureus* (e) after treatments with different groups. The differential lipid cluster analysis and heat map view of *E. coli* (f) and *S. aureus* (g) after treatments with different groups. (Cer: ceramide; PE: phosphatidylethanolamine; PC phosphatidylcholine; PA: phosphatidic acid; TG: triacylglycerol; SM: sphingomyelin).

antibacterial agents (i.e., Cu^{2+} and Cur), we speculated that the antibacterial performance of CuPPSi-Cur could be effectively augmented through combining a mild-temperature (~45 °C) photothermal effect (Figure 4a). Here, common *Escherichia coli* (*E. coli*) and *Staphylococcus aureus* (*S. aureus*) in wound infection were employed as a Gram-negative and a Gram-positive antibacterial model, respectively.[S3,60] As depicted in Figure 4b,c, both *E. coli* and *S. aureus* treated with CuPPSi and CuPPSi-Cur exhibited a significantly decreased viability as compared to those in the control group. Due to the mild-temperature photothermal effect accompanied with the NIR responsive release of an antibacterial agent, CuPPSi and CuPPSi-Cur featured a more prominent bactericidal effect against both kinds of bacteria with the assistance of NIR laser irradiation. For CuPPSi at a concentration of 200 μg/mL, the viability of *E. coli* and *S. aureus* in the absence of NIR irradiation was 59.2% and 54.2%, respectively. Under NIR laser irradiation, more than 75% of bacteria treated with same concentration of CuPPSi was eliminated due to the heat generation by CuPPSi. Furthermore, the bacterial viability in the CuPPSi-Cur treatment group decreased significantly, and the killing rate reached more than 98% at a concentration of 200 μg/mL under NIR laser irradiation. Figure 4d,e shows the images of *E. coli* and *S. aureus* colonies on agar plates in different groups. In control groups, there was no distinct reduction in bacterial colonies no matter whether the NIR irradiation was present or not, indicating that NIR alone could not efficiently kill bacteria without the assistance of photothermal agents. In contrast, CuPPSi and CuPPSi-Cur showed obvious antibacterial performance in bacterial colonies under NIR laser irradiation. These results revealed that the synergistic effect of photothermal induced mild-temperature, CuPPSi carrier, and Cur could be achieved on the CuPPSi-Cur platform for highly effective bacteria killing. The presence of Cu^{2+} on the *E. coli* and *S. aureus* bacterial surfaces after incubation with CuPPSi-Cur was detected by EDS in SEM

https://doi.org/10.1021/acsami.2c12012
ACS Appl. Mater. Interfaces 2022, 14, 48368−48383

observation. As revealed in Figure S8, there was no obvious Cu signal in the bacterial area without NIR irradiation, while a distinct peak of Cu Lα at 0.94 keV could be detected on the surface of bacteria after NIR laser irradiation. The results further confirmed that the PTT effect of the CuPPSi can promote the release of Cu^{2+}.

Unlike planktonic bacteria, the accumulation of aggregated bacterial pathogens in the wound might form a robust biofilm, which reduces the activities of the antibacterial agents and eventually leads to the recurrent infections.[16,60] Encouraged by the excellent antibacterial property of the CuPPSi-Cur nanoplatform, the antibiofilm performance was systematically evaluated by the classic crystal violet staining assays after incubating *E. coli* and *S. aureus* biofilms with different concentrations of CuPPSi-Cur with or without NIR irradiation. As visualized in Figure 4f,g, a dose-dependent behavior of CuPPSi-Cur on the eradication of *E. coli* and *S. aureus* biofilms was observed and the antibiofilm efficiency significantly enhanced with the assistance of NIR laser irradiation. Quantification of the remaining biofilm biomass of both bacteria after treated with different concentrations of CuPPSi-Cur also showed the same trend (Figure 4h,i). The results confirmed that the synergistic effect of the coantibacterial agent and photothermal treatment could eliminate the preformed biofilm more effectively. To further reveal the antibiofilm effect, the morphology of biofilms with different treatments were observed by SEM. As shown in Figure 4j, the biofilms of *S. aureus* and *E. coli* had an integrated cellar morphology and a smooth surface in the control and control + NIR groups. In contrast, treating the biofilm with CuPPSi and CuPPSi-Cur could lead to the collapse of the bacteria surface. In the CuPPSi + NIR and CuPPSi-Cur + NIR treated groups, the biofilm displayed more skeleton collapse, further confirming the synergistic role of released antibacterial agents (Cu^{2+} and Cur) and mild-temperature PTT in the CuPPSi-Cur system under NIR laser irradiation.

2.6. Synergistic and Mild-Temperature Photothermal Augmented Antibacterial Mechanism. To further test the synergistic antibacterial activity, the minimum inhibitory concentrations (MICs) of CuPPSi and Cur were determined, and the results are summarized in Table S1. As shown, the MICs of Cur for *E. coli* and *S. aureus* were 250 and 125 μg/mL, respectively, while the MICs of CuPPSi were measured to be 1500 and 1000 μg/mL for *E. coli* and *S. aureus*, respectively. Both CuPPSi and Cur were more likely to inhibit *S. aureus* proliferation. The synergistic effect between CuPPSi and Cur on bacterial inactivation was quantitatively measured by the combination index (CI) according to previous research.[53] The different CI values represent additive effect (CI = 1), antagonism (CI > 1) and synergism (CI < 1), respectively. As shown in Figure 5a,b, the CI values of the CuPPSi-Cur system were determined to be 0.69 and 0.58 for *E. coli* and *S. aureus*, respectively, indicating the strong synergestic effects between CuPPSi and Cur. The synergistic effect might be ascribed to the increased membrane polarity and destroy of the bacterial cell membrane in the presence of Cur, leading to the improved sensitivity to other antibacterial agents.[33,61] Another possible mechanism involves the binding of Cu^{2+} and Cur that shows higher bioactivity for bacterial killing compared to Cu^{2+} or Cur alone.[62]

The photothermal function of CuPPSi is another important factor for bacterial inhibition. To clarify the dose-dependent behavior of NIR on the antibacterial effect, *E. coli* and *S. aureus* were treated with NIR irradiation for different times in the presence of CuPPSi-Cur (200 μg/mL), and the relative antibacterial efficiencies were tested. As shown in Figure 5c, the *E. coli* and *S. aureus* could be further destroyed under NIR treatment and the antibacterial efficiency improved with the increasing of the irradiation time. This phenomenon might be attributed either to the enhanced release of antibacterial agents or to the increase of bacterial sensitivity to therapeutic agents under an elevated temperature.

It is well-known that bacteria are composed of a variety of lipid types.[63] The bacterial lipid metabolite changes convey much valuable information on the interactions between antibacterial treatment and bacteria.[64,65] Previous reports revealed that the high temperature in conventional PTT could disrupt the enzyme activity and phospholipids on the cell membrane.[66,67] The activity of antibacterial agents also depends on their interaction with bacterial membranes.[62] However, there are few investigations about the change of lipid molecular pattern when treated with different therapy. To further prove the differential antibacterial mechanism of various treatment from a molecular perspective, the lipid metabolite fingerprint of five bacterial groups including Control, CuPPSi treating, Cur treating, CuPPSi-Cur treating, and CuPPSi-Cur plus NIR treating were obtained by a nanostructure-assisted laser desorption/ionization MS technique developed by our group.[68−71] As shown in Figure S9, the MS spectra show the substantial variation in the composition of bacterial membranes after different treatments. The MS data was then analyzed by principal component analysis (PCA). According to the results in Figure 5d,e, we could see the lipid metabolic variabilities of the five groups. The phenotypes of *E. coli* and *S. aureus* under different test groups were clustered into a single quadrant and there was no overlap of the cluster with each other in the 2D PCA space, demonstrating the different antibacterial mechanisms of the five groups. Moreover, S-plot and *t* test were conducted to discover feature lipid biomarkers. Accordingly, 10 and 11 lipids with *P* values <0.0001 and variable importance in projection (VIP) scores >1 were selected as the feature lipids with identified structure for *E. coli* and *S. aureus*, respectively. (Tables S2 and S3). As suggested by identified lipid species, the feature phospholipids of *E. coli* and *S. aureus* were predominantly phosphatidyl cholines (PCs) and phosphatidyl ethanolamines, which is consistent with previous research.[72,73] Using these feature lipid biomarkers, hierarchical clustering analysis (HCA) results showed that each type of treatment for *E. coli* and *S. aureus* can be classified into their corresponding groups (Figure 5f,g). The results suggested that lipids responsible for metabolism regulation in the *E. coli* and *S. aureus* strains were disturbed by the different antibacterial treatments. The dramatically different expression patterns of the five treatment groups are the result of combined actions of multiple factors including drug, carrier (CuPPSi), and low-temperature PTT. The study also indicated that the pattern of lipid peak panel can be applied to reveal drug response of bacteria at a molecular level. The strategy is a valuable attempt to provide more clues to reveal the killing mechanisms of the different antibacterial treatments. In the future study, a deeper study combining genome analysis needs to be investigated to elucidate the specific metabolic pathways of the antibacterial mechanisms.

2.7. Hemocompatibility, Cytocompatibility, and Cell Scratch Healing Evaluation. After implantation *in vivo*, biomaterials were in contact with blood directly. Therefore,

https://doi.org/10.1021/acsami.2c12012
ACS Appl. Mater. Interfaces 2022, 14, 48368−48383

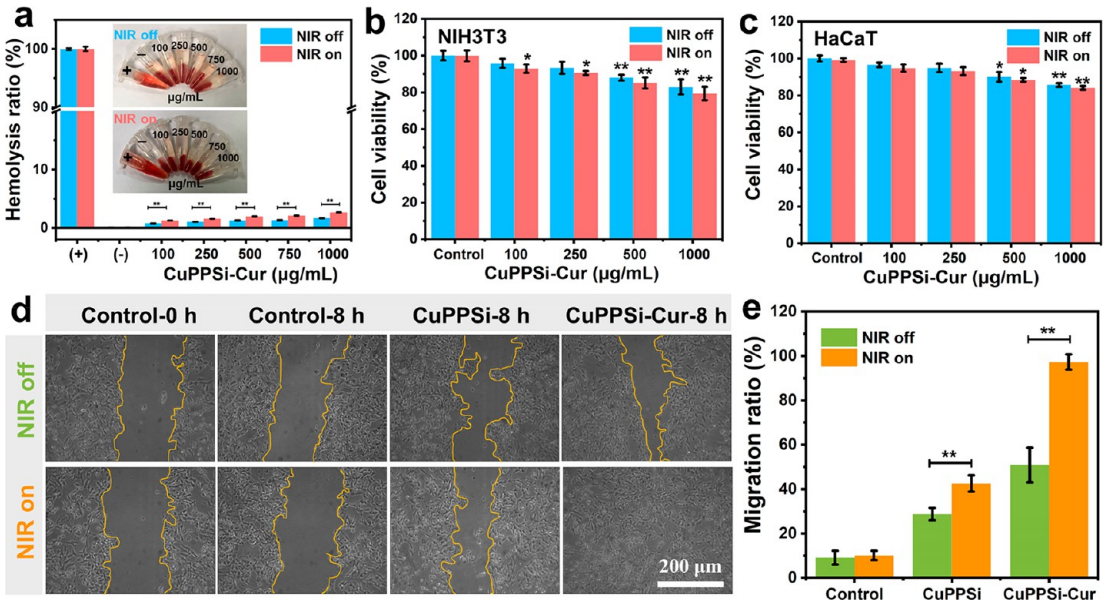

Figure 6. (a) Hemolysis rate of CuPPSi-Cur particles with or without NIR laser irradiation at various concentrations. Inset shows the photograph of different samples. Deionized water and PBS were employed as positive (+) and negative controls (−), respectively. The NIH3T3 (b) and HaCaT cell (c) viabilities after treated with various concentrations of CuPPSi-Cur with or without NIR laser irradiation for 48 h. * means $p < 0.05$, and ** means $p < 0.01$ compared to control, $n = 3$. (d) Images of the scratch assay of NIH3T3 cells after treated with different groups (Control, CuPPSi, CuPPSi-Cur) with or without NIR laser irradiation for 8 h. (e) The quantitative analysis of NIH3T3 cells migration ratio for 8 h. The error bars represent mean ± SD (**$p < 0.01$, $n = 3$).

hemolysis caused by materials is a necessary consideration for further biomedical use. The hemolytic property of CuPPSi-Cur particles on human erythrocytes was tested with or without NIR laser irradiation. As shown in Figure 6a, all test groups presented very low hemolysis rates (<3%), indicating that CuPPSi-Cur + NIR is biosafe for blood-contacting applications. Further cytotoxicities of the CuPPSi-Cur particles were assessed via NIH3T3 and HaCaT cells, two kinds of typical skin cells. As revealed in Figure 6b,c, all the examined cells exhibited high viability (>80% survival ratio) after treated with CuPPSi-Cur at 100−1000 μg/mL concentrations for 48 h. The viability of NIH3T3 and HaCaT cells incubated with CuPPSi-Cur upon NIR irradition remained at a high level and exhibited no obvious difference in comparison to the NIR off group. Furthermore, the cytocompatibility of CuPPSi-Cur under the cyclic exposure to NIR light was also evaluated. After NIR laser irradiation for 3 cycles, all cells still displayed good viability in comparison to control sample, even the concentration of CuPPSi-Cur reached 500 μg/mL (Figure S10). All the results confirmed the biocompatibility and biosafety of the CuPPSi-Cur platform with NIR-triggered mild PTT (~45 °C).

According to previous reports, fibroblasts migration is a significant process for wound healing.[26,29] Here, the effect of released ions and drugs from CuPPSi-Cur on NIH3T3 cells migration was evaluated by typical scratch assays. As shown in Figure 6d,e, the CuPPSi showed faster scratch healing with an approximately 2.7-fold migration rate in comparison to the control group. The results might be attributed to the promotion effect of released Cu and Si ions on NIH3T3 cells migration.[29,30] In addition, the scratch region treated with CuPPSi-Cur was narrower than that of CuPPSi due to the effect of the Cur payload.[74−76] Notably, the cells treated with CuPPSi-Cur + NIR showed the highest migration capability because NIR light triggered the release of more therapeutic agents including Cur (1.84% of initial amount of payload) and Cu^{2+} (6.92 ppm). These results reveal that the NIR-irradiated CuPPSi-Cur not only has negligible cytotoxicity but also promotes the function of cell migrating. The results also confirmed that the inherent deficiencies such as thermoresistance and overheating damage of conventional PTT have been avoided. Overall, the CuPPSi-Cur combined with mild-temperature PTT exhibits high antibacterial efficiency, low cytotoxicity, as well as a promotion effect on cell migrating.

2.8. *In Vivo* Wound Healing and Disinfection. As mentioned above, the CuPPSi-Cur platform not only improves the stability and bioavailability of Cur but also realizes multi-stimuli-responsive drug release under the stimulation of pH, ROS, and NIR for on-demand delivery as well as mild PTT-augmented antibacterial therapy. Motivated by the high antibacterial performance and good cytocompatibility of CuPPSi-Cur *in vitro*, the *in vivo* anti-infection performance of CuPPSi-Cur on cutaneous wound healing by a *S. aureus*-infected mice model was conducted (Figure 7a). The photothermal performance of a CuPPSi-based mild-temperature PTT platform was first assessed *in vivo*. As shown in Figure S11, after 5 min of NIR irradiation with the power density at 0.33 W/cm^2 (the American National Standard for biosafe application *in vivo*),[77] the wound region temperature of CuPPSi and CuPPSi-Cur was raised to ~45 °C, while the local temperature of the PBS + NIR groups was only enhanced to ~39 °C under the same conditions. Representative photographs of wound after different treatments on Day 0, Day 2, Day 4, and Day 7 are shown in Figure 7b and the corresponding statistical results are summarized in Figure 7c. After a one-week treatment, the wound area in the PBS and PBS + NIR groups reduced to 61.3% and 62.3%, respectively. After treatment with CuPPSi for the same days, the remaining wound area reduced to 35.2% owing to therapeutic effect of released ions from the CuPPSi carrier. If treated with the CuPPSi + NIR group (~45 °C), the area of infected wound

https://doi.org/10.1021/acsami.2c12012
ACS Appl. Mater. Interfaces 2022, 14, 48368−48383

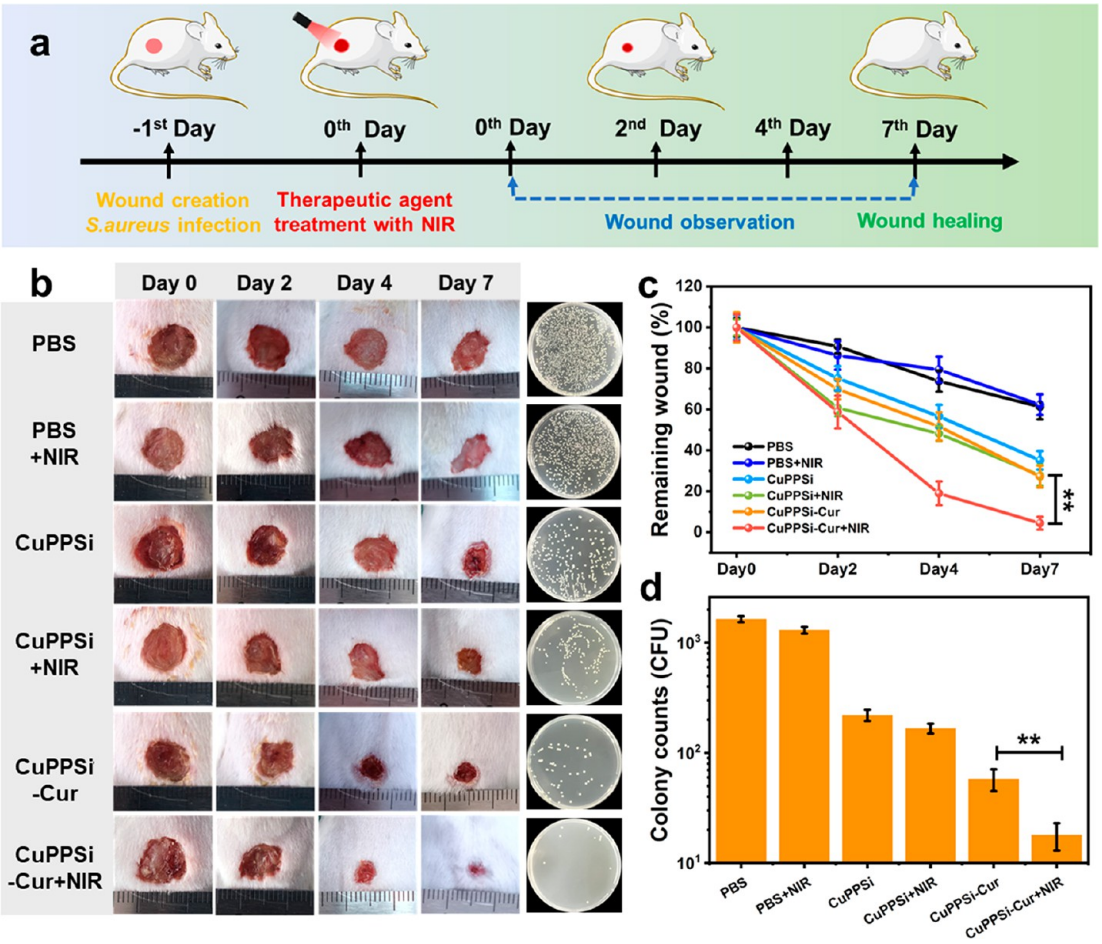

Figure 7. (a) Schematic illustration of *S. aureus*-infected wound creation and healing process. (b) Photographs of *S. aureus*-infected wounds and grown bacteria colonies incubated on agar plates after various different. (c) Corresponding statistics of remaining wound area at 0, 2, 4, and 7 days in the six different treatment groups. (d) The statistical data of colonies of *S. aureus* in the skin wound at Day 7. The error bars represent mean ± SD (**$p < 0.01$, $n = 3$).

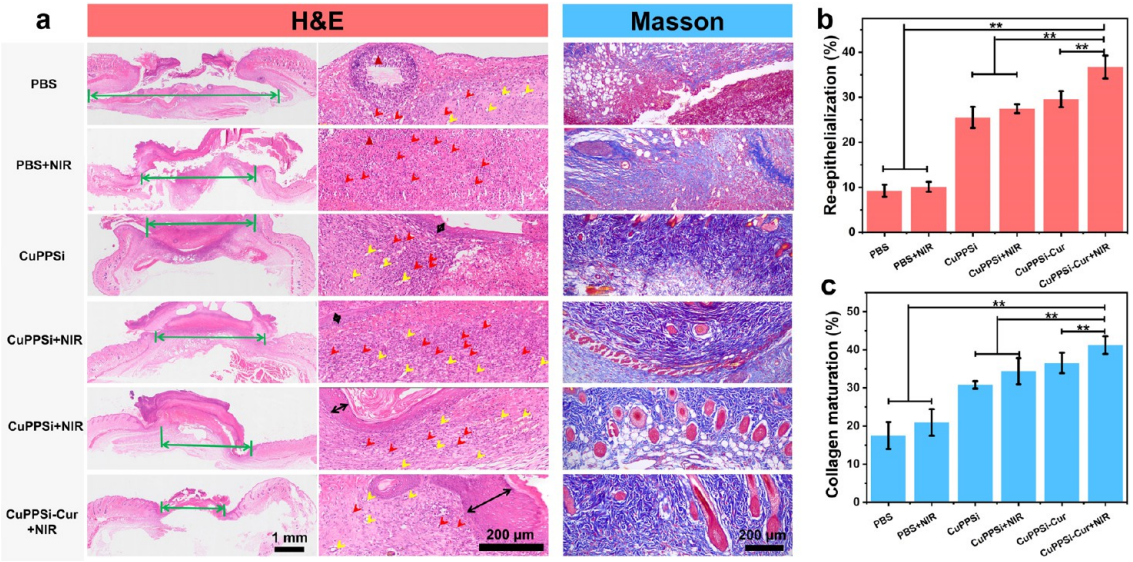

Figure 8. (a) Representative H&E staining and Masson's trichrome staining results of the skin wound tissues at Day 7 (green arrow: unclosed wound width, red arrow: inflammatory cell infiltrate, yellow arrow: blood vessels, black arrow: regenerated epidermis). Quantification of re-epithelialization from H&E staining (b) and collagen maturation from Masson's trichrome staining (c). The error bars represent mean ± SD (**$p < 0.01$, $n = 3$).

https://doi.org/10.1021/acsami.2c12012
ACS Appl. Mater. Interfaces 2022, 14, 48368−48383

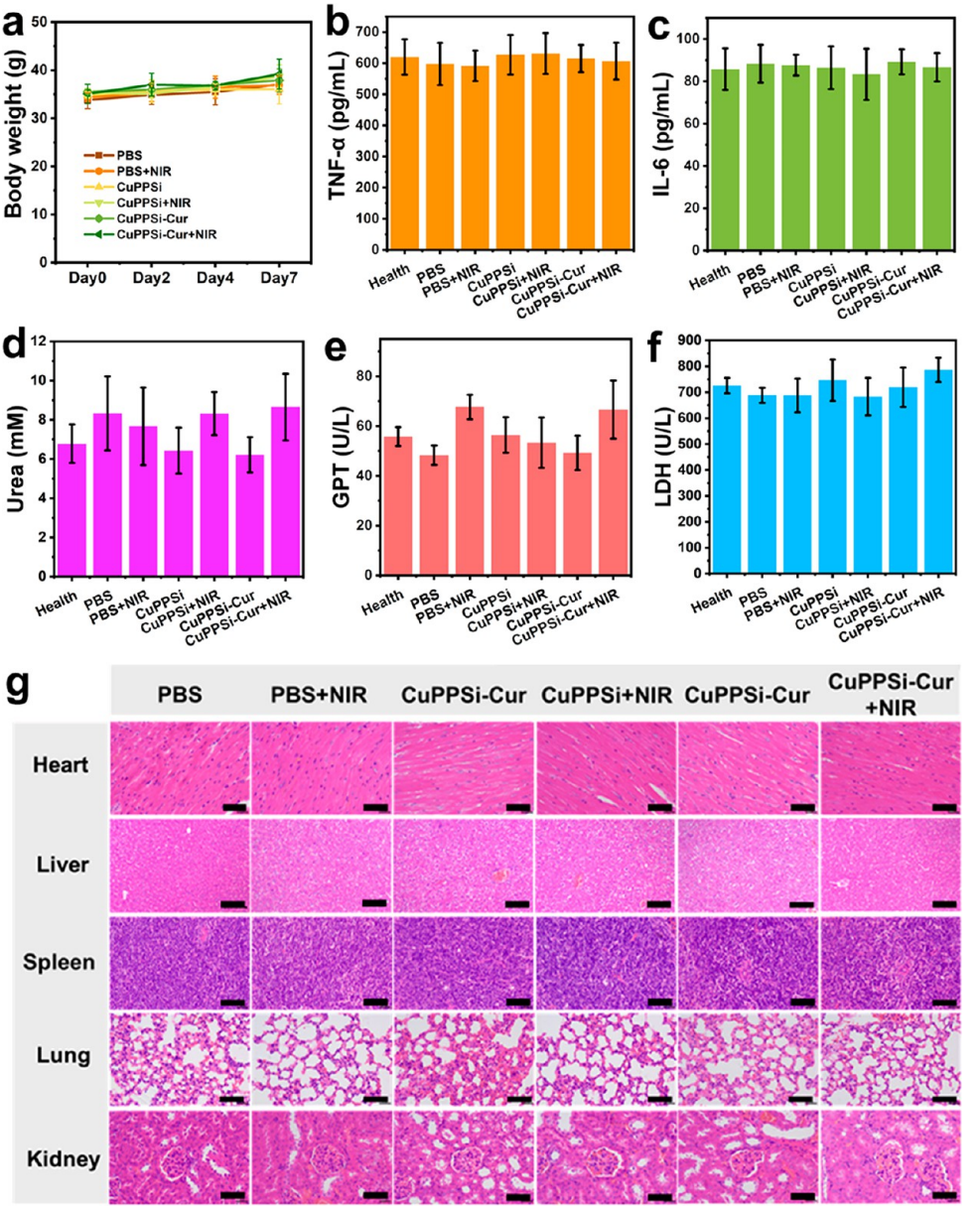

Figure 9. (a) Body weight changes of the mice after different treatments on Day 0, Day 2, Day 4, and Day 7. Levels of IL-6 (b), TNF-α (c), urea (d), GPT (e), and LDH(f) after 7 days of different treatments. The error bars represent mean ± SD (**$p < 0.01$, $n = 3$). (d) H&E staining images of the heart, liver, spleen, lung, and kidney tissues after 7 days of treatment. The scale bars are 100 μm.

reduced to 27.8% of the original wound with fewer colonies of bacteria, showing the enhanced wound healing and antibacterial effect. In the CuPPSi-Cur treatment group, the wound area decreased to 27.2% owing to the on-demand and synergistic treatment efficacy of CuPPSi and Cur. Under the NIR assistance, more than 95% of wound area was closed, indicating the synergistic effect of mild PTT and coantibacterial agent could outstandingly improve the ability of wound healing. The mild PTT strategy not only inhibits bacteria growth in wound area but also avoid the nearby normal tissues from damaging. Additionally, the plate count results of *S. aureus* incubation suggested that the wound treated with PBS and PBS + NIR exhibited high bacterial density, while the bacterial colony numbers slightly decreased if the wound was treated with CuPPSi and CuPPSi-Cur (Figure 7b,d). In contrast, CuPPSi-Cur + NIR treatment exhited the strongest wound disinfection effect, further proving that the synergestic effect of combined therapy. For comparison, Table S4 lists some studies that were used to deliver Cur for wound disinfection. Obviously, the present CuPPSi-Cur system is more superior because it can achieve multistimuli-responsive drug release (pH, ROS, and NIR), codelivery of two-component agents (Cu^{2+} and Cur) as well as mild PTT-augmented efficacy for synergistic and amplified bacteria-infected wound therapy *in vivo*.

2.9. *In Vivo* Histological and Biosafety Analysis. To further evaluate the quality of regenerated skin in wound defects among the six groups, histological staining assays were performed by hematoxylin and eosin (H&E) staining and Masson's trichrome staining on Day 7. As analyzed in the H&E staining results, serious dermis layer damage and inflammatory cell infiltration in the PBS and PBS + NIR groups was found as marked with red-colored arrows in Figure 8a, demonstrating the seriousness of the infected wound and the poor healing

https://doi.org/10.1021/acsami.2c12012
ACS Appl. Mater. Interfaces 2022, 14, 48368−48383

ability. After treatment, the infected skin tissues showed a relative intact histological characteristic. Narrower unclosed wound width (indicated with green-colored arrows), new vessels (indicated with yellow-colored arrows), a thicker dermis layer (indicated with black-colored arrows) and less inflammation could be observed in the CuPPSi-Cur and CuPPSi-Cur + NIR groups. The re-epithelialization as well as the formation of collagen is essential for the skin tissue regeneration during wound healing. As calculated from the H&E staining, both CuPPSi treatment and CuPPSi-Cur increased the re-epithelialization of the wound bed area from ∼10% in the PBS and PBS + NIR groups to ∼25% and ∼30% in the CuPPSi + NIR and CuPPSi-Cur + NIR groups, respectively (Figure 8b). By quantitative analysis of Masson's trichrome staining (Figure 8c), collagen maturation was significantly higher in the CuPPSi-Cur + NIR group (41.24 ± 2.33%) than in the CuPPSi-Cur group (36.55 ± 2.67%) and other groups (PBS without/with NIR and CuPPSi without/with NIR), which further supports that CuPPSi-Cur + NIR is an effective integrated therapy for accelerating skin wound-healing process through promoting re-epithelialization as well as collagen maturation.

Next, the assessment of biological safety for different treatments was performed.The stable body weight of the mice initially shows that the group treated with CuPPSi-Cur + NIR had no apparent histological toxicology (Figure 9a), indicating the biosafety for *in vivo* application. Furthermore, blood analysis was performed on Day 7 to study the biotoxicity of the different treatments. As revealed in Figure S12, there was no significant difference between healthy and experimental groups in the values of white red blood cell (RBC), blood cell (WBC), hematocrit (HCT), hemoglobin (HGB), platelet (PLT), mean corpuscular volume (MCV), and mean corpuscular hemoglobin (MCHC), suggesting no acute toxicity was caused by the different treatments. The proinflammatory responses after different therapeutic systems were evaluated by measuring the levels of the inflammatory cytokines interleukin-6 (IL-6) and tumor necrosis factor-α (TNF-α) in serum (Figure 9b,c). The results showed that all the treatment caused no inflammatory response, suggesting that the therapeutic platform does not cause undesirable tissue immunotoxic reactions and systemic toxicity. To further study the potential toxicology of the treatments on major organs, the blood chemistry indexes including urea (sign of kidney function), glutamic-pyruvic transaminase (GPT, sign of liver function), and lactate dehydrogenase (LDH, sign of lung function) were examined. As shown in Figure 9d−f, there was no significance in urea, GPT, and LDH levels between healthy (untreated mice) and treated groups, which indicated that the novel DDS platform developed in this work would not damage the kidney, liver, and lung function of mice.

Besides, the *in vivo* biocompatibility and biological biosafety of different groups was also evaluated by H&E staining of major organs after wound treatment on Day 7. As indicated in Figure 9g, no obvious inflammatory cell infiltration or damage on the major organs (heart, liver, spleen, lung, and kidney) were observed. The accumulation of Si and Cu in major organs, healed wound, and skin tissue on the seventh day of CuPPSi-Cur + NIR treatment was further determined by ICP-OES. As indicated in Figure S13, most Si and Cu elements located at the wound area but extremely low in skin tissue (<60 ng/g) or major organs (<6 ng/g). The results conclude that the released ions rarely enter into blood and participate in the whole-body metabolism, supporting the safety of CuPPSi-Cur + NIR in wound treatment.

3. CONCLUSIONS

In summary, with a simple and fast surface reduction-induced deposition strategy, CuPDA coating has been successfully modified on the PSi drug vehicle, which is endowed with significant photothermal and therapeutic effects. Meanwhile, the PSi carrier retains its porous structure and possesses more abundant surface groups, enabling loading and interplay with drugs more efficiently. The release of therapeutic components including degraded ions and Cur payload can be stimulated by wound internal factors (pH and ROS) and external NIR laser irradition. More importantly, the integration of PTT further enhances the bactericidal effect of the CuPPSi-Cur system for combating *E. coli* and *S. aureus*, and even their biofilms. Compared to the commonly used drug carriers, the PSi endowed with photothermal and therapeutic effects not only allows ion degradation and drug release in a thermal-stimuli manner but also enhances synergistic bacteriacidal activity with drug payloads under a mild PTT temperature (∼45 °C). In addition, the CuPPSi-mediated mild-temperature PTT used in this work reduces the overheating damage to normal cells/tissues and synergistically amplifies wound disinfection effects under biosafe conditions. The potential of the PSi carrier endowed with photothermal and therapeutic effects is promising to broaden the scope of porous materials' applications in biomedicine, and expected to be further expanded in the clinical practice.

■ ASSOCIATED CONTENT

Supporting Information

The Supporting Information is available free of charge at https://pubs.acs.org/doi/10.1021/acsami.2c12012.

Experimental section; further characterization data of CuPPSi including SEM, EDS, and XPS; UV−vis absorption spectrum, photos and the working curve for Cur; DR-FTIR spectrum of CuPPSi and CuPPSi-Cur; comparison of the antioxidant activity; Si ions release; SEM images, corresponding EDS patterns and typical mass spectra of bacteria after treatment; cell viabilities of CuPPSi-Cur after NIR irradiation exposure in the cyclic fashion; photothermal curves and images of infected mice with different treatments; complete blood panel analysis; the Si and Cu content accumulated in major organs; MIC values of Cur, CuPPSi and CuPPSi-Cur; putative identification of biomarkers for bacteria and comparison of different Cur delivery systems (PDF)

■ AUTHOR INFORMATION

Corresponding Authors

Yongke Zheng − *Department of Intensive Care Unit, Affiliated Hangzhou First People's Hospital, Zhejiang University School of Medicine, Hangzhou 310006, China*; Email: zyk97091@163.com

Jianmin Wu − *Lab of Nanomedicine and Omic-based Diagnostics, Institute of Analytical Chemistry, Department of Chemistry, Zhejiang University, Hangzhou 310058, China*; orcid.org/0000-0002-0999-9194; Email: wjm-st1@zju.edu.cn

https://doi.org/10.1021/acsami.2c12012
ACS Appl. Mater. Interfaces 2022, 14, 48368−48383

Authors

Wei Duan − *Lab of Nanomedicine and Omic-based Diagnostics, Institute of Analytical Chemistry, Department of Chemistry, Zhejiang University, Hangzhou 310058, China;* orcid.org/0000-0002-6609-1043

Xingyue Liu − *Lab of Nanomedicine and Omic-based Diagnostics, Institute of Analytical Chemistry, Department of Chemistry, Zhejiang University, Hangzhou 310058, China*

Jingwen Zhao − *Lab of Nanomedicine and Omic-based Diagnostics, Institute of Analytical Chemistry, Department of Chemistry, Zhejiang University, Hangzhou 310058, China*

Complete contact information is available at: https://pubs.acs.org/10.1021/acsami.2c12012

Author Contributions

The paper was written through contributions of all authors. J.W. conceived the project and supervised the research. W.D. and X.L. designed and performed the experiments. W.D., X.L., J.Z., and Y.Z. discussed the data and checked the paper. W.D. and J.W. wrote the paper. All authors give approval to the final version of the paper.

Notes

The authors declare no competing financial interest.

■ ACKNOWLEDGMENTS

We acknowledge the financial support from the National Natural Science Foundation of China (Nos. 21575127 and 21874118). We also highly appreciated the mass spectrometry detection and data analysis supported by the Well-healthcare Technologies Co., LTD (Hangzhou, China).

■ REFERENCES

(1) Rendeiro, A. F.; Ravichandran, H.; Bram, Y.; Chandar, V.; Kim, J.; Meydan, C.; Park, J.; Foox, J.; Hether, T.; Warren, S.; Kim, Y.; Reeves, J.; Salvatore, S.; Mason, C. E.; Swanson, E. C.; Borczuk, A. C.; Elemento, O.; Schwartz, R. E. The Spatial Landscape of Lung Pathology During COVID-19 Progression. *Nature* **2021**, *593* (7860), 564−569.

(2) Torales, J.; O'Higgins, M.; Castaldelli-Maia, J. M.; Ventriglio, A. The Outbreak of COVID-19 Coronavirus and Its Impact on Global Mental Health. *International Journal of Social Psychiatry* **2020**, *66* (4), 317−320.

(3) Hutchings, M. I.; Truman, A. W.; Wilkinson, B. Antibiotics: Past, Present and Future. *Curr. Opin. Microbiol.* **2019**, *51*, 72−80.

(4) Hamad, B. The Antibiotics Market. *Nat. Rev. Drug Discovery* **2010**, *9* (9), 675.

(5) Wang, Y.; Yang, Y.; Shi, Y.; Song, H.; Yu, C. Antibiotic-Free Antibacterial Strategies Enabled by Nanomaterials: Progress and Perspectives. *Adv. Mater.* **2020**, *32* (18), 1904106.

(6) Taylor, P. W. Alternative Natural Sources for a New Generation of Antibacterial Agents. *Int. J. Antimicrob. Agents* **2013**, *42* (3), 195−201.

(7) Czaplewski, L.; Bax, R.; Clokie, M.; Dawson, M.; Fairhead, H.; Fischetti, V. A.; Foster, S.; Gilmore, B. F.; Hancock, R. E.; Harper, D. Alternatives to Antibiotics—A Pipeline Portfolio Review. *Lancet Infect. Dis.* **2016**, *16* (2), 239−251.

(8) Wang, S.; Zeng, X.; Yang, Q.; Qiao, S. Antimicrobial Peptides as Potential Alternatives to Antibiotics in Food Animal Industry. *International Journal of Molecular Sciences* **2016**, *17* (5), 603.

(9) Kim, T.; Zhang, Q.; Li, J.; Zhang, L.; Jokerst, J. V. A Gold/Silver Hybrid Nanoparticle for Treatment and Photoacoustic Imaging of Bacterial Infection. *ACS Nano* **2018**, *12* (6), 5615−5625.

(10) GhavamiNejad, A.; Rajan Unnithan, A.; Ramachandra Kurup Sasikala, A.; Samarikhalaj, M.; Thomas, R. G.; Jeong, Y. Y.; Nasseri, S.; Murugesan, P.; Wu, D.; Hee Park, C.; Kim, C. S. Mussel-Inspired Electrospun Nanofibers Functionalized with Size-Controlled Silver Nanoparticles for Wound Dressing Application. *ACS Appl. Mater. Interfaces* **2015**, *7* (22), 12176−12183.

(11) Jahan, I.; George, E.; Saxena, N.; Sen, S. Silver-Nanoparticle-Entrapped Soft GelMA Gels as Prospective Scaffolds for Wound Healing. *ACS Applied Bio Materials* **2019**, *2* (5), 1802−1814.

(12) Canaparo, R.; Foglietta, F.; Giuntini, F.; Della Pepa, C.; Dosio, F.; Serpe, L. Recent Developments in Antibacterial Therapy: Focus on Stimuli-Responsive Drug-Delivery Systems and Therapeutic Nanoparticles. *Molecules* **2019**, *24* (10), 1991.

(13) Chen, H.; Jin, Y.; Wang, J.; Wang, Y.; Jiang, W.; Dai, H.; Pang, S.; Lei, L.; Ji, J.; Wang, B. Design of Smart Targeted and Responsive Drug Delivery Systems with Enhanced Antibacterial Properties. *Nanoscale* **2018**, *10* (45), 20946−20962.

(14) Tang, N.; Zhang, R.; Zheng, Y.; Wang, J.; Khatib, M.; Jiang, X.; Zhou, C.; Omar, R.; Saliba, W.; Wu, W.; Yuan, M.; Cui, D.; Haick, H. Highly Efficient Self-Healing Multifunctional Dressing with Antibacterial Activity for Sutureless Wound Closure and Infected Wound Monitoring. *Adv. Mater.* **2022**, *34* (3), 2106842.

(15) Cheng, J.; Gan, G.; Shen, Z.; Gao, L.; Zhang, G.; Hu, J. Red Light-Triggered Intracellular Carbon Monoxide Release Enables Selective Eradication of MRSA Infection. *Angew. Chem., Int. Ed.* **2021**, *60* (24), 13513−13520.

(16) Hu, D.; Li, H.; Wang, B.; Ye, Z.; Lei, W.; Jia, F.; Jin, Q.; Ren, K.-F.; Ji, J. Surface-Adaptive Gold Nanoparticles with Effective Adherence and Enhanced Photothermal Ablation of Methicillin-Resistant Staphylococcus Aureus Biofilm. *ACS Nano* **2017**, *11* (9), 9330−9339.

(17) Mao, D.; Hu, F.; Ji, S.; Wu, W.; Ding, D.; Kong, D.; Liu, B. Metal−Organic-Framework-Assisted in vivo Bacterial Metabolic Labeling and Precise Antibacterial Therapy. *Adv. Mater.* **2018**, *30* (18), 1706831.

(18) Mura, S.; Nicolas, J.; Couvreur, P. Stimuli-Responsive Nanocarriers for Drug Delivery. *Nat. Mater.* **2013**, *12* (11), 991−1003.

(19) Mi, P. Stimuli-Responsive Nanocarriers for Drug Delivery, Tumor Imaging. *Therapy and Theranostics. Theranostics* **2020**, *10* (10), 4557.

(20) Zhao, W.; Zhao, Y.; Wang, Q.; Liu, T.; Sun, J.; Zhang, R. Remote Light-Responsive Nanocarriers for Controlled Drug Delivery: Advances and perspectives. *Small* **2019**, *15* (45), 1903060.

(21) Guan, G.; Win, K. Y.; Yao, X.; Yang, W.; Han, M. Y. Plasmonically Modulated Gold Nanostructures for Photothermal Ablation of Bacteria. *Adv. Healthcare Mater.* **2021**, *10* (3), 2001158.

(22) Cao, Y.; Wu, T.; Zhang, K.; Meng, X.; Dai, W.; Wang, D.; Dong, H.; Zhang, X. Engineered Exosome-Mediated Near-Infrared-II Region V2C Quantum Dot Delivery for Nucleus-Target Low-Temperature Photothermal Therapy. *ACS Nano* **2019**, *13* (2), 1499−1510.

(23) Cui, X.; Liang, Z.; Lu, J.; Wang, X.; Jia, F.; Hu, Q.; Xiao, X.; Deng, X.; Wu, Y.; Sheng, W. A Multifunctional Nanodiamond-Based Nanoplatform for The Enhanced Mild-Temperature Photothermal/Chemo Combination Therapy of Triple Negative Breast Cancer via an Autophagy Regulation Strategy. *Nanoscale* **2021**, *13* (31), 13375−13389.

(24) Park, J.-H.; Gu, L.; Von Maltzahn, G.; Ruoslahti, E.; Bhatia, S. N.; Sailor, M. J. Biodegradable Luminescent Porous Silicon Nanoparticles for In Vivo Applications. *Nat. Mater.* **2009**, *8* (4), 331−336.

(25) Kang, J.; Joo, J.; Kwon, E. J.; Skalak, M.; Hussain, S.; She, Z. G.; Ruoslahti, E.; Bhatia, S. N.; Sailor, M. J. Self-Sealing Porous Silicon-Calcium Silicate Core−Shell Nanoparticles for Targeted siRNA Delivery to The Injured Brain. *Adv. Mater.* **2016**, *28* (36), 7962−7969.

(26) Cui, Y.; Duan, W.; Jin, Y.; Wo, F.; Xi, F.; Wu, J. Graphene Quantum Dot-Decorated Luminescent Porous Silicon Dressing for Theranostics of Diabetic Wounds. *Acta Biomaterialia* **2021**, *131*, 544−554.

(27) Jung, Y.; Huh, Y.; Kim, D. Recent Advances in Surface Engineering of Porous Silicon Nanomaterials for Biomedical Applications. *Microporous Mesoporous Mater.* **2021**, *310*, 110673.
(28) Cai, S. S.; Li, T.; Akinade, T.; Zhu, Y.; Leong, K. W. Drug Delivery Carriers with Therapeutic Functions. *Adv. Drug Delivery Rev.* **2021**, *176*, 113884.
(29) Duan, W.; Jin, Y.; Cui, Y.; Xi, F.; Liu, X.; Wo, F.; Wu, J. A Co-Delivery Platform for Synergistic Promotion of Angiogenesis Based on Biodegradable, Therapeutic and Self-Reporting Luminescent Porous Silicon Microparticles. *Biomaterials* **2021**, *272*, 120772.
(30) Ermini, M. L.; Voliani, V. Antimicrobial Nano-Agents: The Copper Age. *ACS Nano* **2021**, *15* (4), 6008−6029.
(31) Jin, A.; Wang, Y.; Lin, K.; Jiang, L. Nanoparticles Modified by Polydopamine: Working as "drug" Carriers. *Bioactive Materials* **2020**, *5* (3), 522−541.
(32) Akbik, D.; Ghadiri, M.; Chrzanowski, W.; Rohanizadeh, R. Curcumin as a Wound Healing Agent. *Life Sciences* **2014**, *116* (1), 1−7.
(33) Mohanty, C.; Sahoo, S. K. Curcumin and Its Topical Formulations for Wound Healing Applications. *Drug Discovery Today* **2017**, *22* (10), 1582−1592.
(34) Chen, X.; Wo, F.; Jin, Y.; Tan, J.; Lai, Y.; Wu, J. Drug-Porous Silicon Dual Luminescent System for Monitoring and Inhibition of Wound Infection. *ACS Nano* **2017**, *11* (8), 7938−7949.
(35) Cui, Y.; Duan, W.; Jin, Y.; Wo, F.; Xi, F.; Wu, J. Ratiometric Fluorescent Nanohybrid for Noninvasive and Visual Monitoring of Sweat Glucose. *ACS Sensors* **2020**, *5* (7), 2096−2105.
(36) Ding, Y.; Floren, M.; Tan, W. Mussel-Inspired Polydopamine for Bio-Surface Functionalization. *Biosurface and Biotribology* **2016**, *2* (4), 121−136.
(37) Cheng, W.; Zeng, X.; Chen, H.; Li, Z.; Zeng, W.; Mei, L.; Zhao, Y. Versatile Polydopamine Platforms: Synthesis and Promising Applications for Surface Modification and Advanced Nanomedicine. *ACS Nano* **2019**, *13* (8), 8537−8565.
(38) Liu, M.; Zeng, G.; Wang, K.; Wan, Q.; Tao, L.; Zhang, X.; Wei, Y. Recent Developments in Polydopamine: an Emerging Aoft Matter for Surface Modification and Biomedical Applications. *Nanoscale* **2016**, *8* (38), 16819−16840.
(39) Xie, X.; Tang, J.; Xing, Y.; Wang, Z.; Ding, T.; Zhang, J.; Cai, K. Intervention of Polydopamine Assembly and Adhesion on Nanoscale Interfaces: State-of-the-Art Designs and Biomedical Applications. *Adv. Healthcare Mater.* **2021**, *10* (9), 2002138.
(40) Bernsmann, F.; Ball, V.; Addiego, F.; Ponche, A.; Michel, M.; Gracio, J. J. d. A.; Toniazzo, V.; Ruch, D. Dopamine− Melanin Film Deposition Depends on the Used Oxidant and Buffer Solution. *Langmuir* **2011**, *27* (6), 2819−2825.
(41) Huang, L.; Jiao, S.; Li, M. Determination of Uric Acid in Human Urine by Eliminating Ascorbic Acid Interference on Copper (II)-Polydopamine Immobilized Electrode Surface. *Electrochim. Acta* **2014**, *121*, 233−239.
(42) Jin, Y.; Duan, W.; Wo, F.; Wu, J. Two-Dimensional Fluorescent Strategy Based on Porous Silicon Quantum Dots for Metal-Ion Detection and Recognition. *ACS Applied Nano Materials* **2019**, *2* (10), 6110−6115.
(43) Jia, X.; Huang, J.; Li, Y.; Yang, J.; Song, H. Monodisperse Cu Nanoparticles@ MoS_2 Nanosheets as a Lubricant Additive for Improved Tribological Properties. *Appl. Surf. Sci.* **2019**, *494*, 430−439.
(44) Zhen, W.; Jiao, W.; Wu, Y.; Jing, H.; Lu, G. The Role of a Metallic Copper Interlayer During Visible Photocatalytic Hydrogen Generation Over a $Cu/Cu_2O/Cu/TiO_2$ Catalyst. *Catalysis Science & Technology* **2017**, *7* (21), 5028−5037.
(45) Wang, A.; Zhang, M.; Yin, H.; Liu, S.; Liu, M.; Hu, T. Direct Reaction Between Silicon and Methanol Over Cu-based Catalysts: Investigation of Active Species and Regeneration of CuCl Catalyst. *RSC Adv.* **2018**, *8* (34), 19317−19325.
(46) Ma, C.; Yang, Z.; Wang, W.; Zhang, M.; Hao, X.; Zhu, S.; Chen, S. Fabrication of Ag−Cu 2 O/PANI Nanocomposites for Visible-Light Photocatalysis Triggering Super Antibacterial Activity. *Journal of Materials Chemistry C* **2020**, *8* (8), 2888−2898.
(47) Fan, H.; Yu, X.; Liu, Y.; Shi, Z.; Liu, H.; Nie, Z.; Wu, D.; Jin, Z. Folic Acid−Polydopamine Nanofibers Show Enhanced Ordered-Stacking via $\pi-\pi$ Interactions. *Soft Matter* **2015**, *11* (23), 4621−4629.
(48) Wu, L.; Gao, Y.; Zhao, C.; Huang, D.; Chen, W.; Lin, X.; Liu, A.; Lin, L. Synthesis of Curcumin-Quaternized Carbon Quantum Dots with Enhanced Broad-Spectrum Antibacterial Activity for Promoting Infected Wound Healing. *Biomaterials Advances* **2022**, *133*, 112608.
(49) Liu, F.; Lin, L.; Zhang, Y.; Sheng, S.; Wang, Y.; Xu, C.; Tian, H.; Chen, X. Two-Dimensional Nanosheets with High Curcumin Loading Content for Multimodal Imaging-Guided Combined Chemo-Photothermal Therapy. *Biomaterials* **2019**, *223*, 119470.
(50) Moballegh Nasery, M.; Abadi, B.; Poormoghadam, D.; Zarrabi, A.; Keyhanvar, P.; Khanbabaei, H.; Ashrafizadeh, M.; Mohammadinejad, R.; Tavakol, S.; Sethi, G. Curcumin Delivery Mediated by Bio-Based Nanoparticles: a Review. *Molecules* **2020**, *25* (3), 689.
(51) Pan, H.; Shen, X.; Tao, W.; Chen, S.; Ye, X. Fabrication of Polydopamine-Based Curcumin Nanoparticles for Chemical Stability and pH-Responsive Delivery. *J. Agric. Food Chem.* **2020**, *68* (9), 2795−2802.
(52) Ak, T.; Gülçin, İ. Antioxidant and Radical Scavenging Properties of Curcumin. *Chemico-Biological Interactions* **2008**, *174* (1), 27−37.
(53) Jin, Y.; Yang, Y.; Duan, W.; Qu, X.; Wu, J. Synergistic and on-Demand Release of Ag-AMPs Loaded on Porous Silicon Nanocarriers for Antibacteria and Wound Healing. *ACS Appl. Mater. Interfaces* **2021**, *13* (14), 16127−16141.
(54) Anglin, E. J.; Cheng, L.; Freeman, W. R.; Sailor, M. J. Porous Silicon in Drug Delivery Devices and Materials. *Adv. Drug Delivery Rev.* **2008**, *60* (11), 1266−1277.
(55) Wang, Z.; Liu, X.; Duan, Y.; Huang, Y. Infection Microenvironment-Related Antibacterial Nanotherapeutic Strategies. *Biomaterials* **2022**, *280*, 121249.
(56) He, Z.; Liu, Y.; Wang, H.; Wang, J.; Pei, X.; Chen, J.; Zhang, X.; Zhu, Z.; Wan, Q. Logic-Based Diagnostic and Therapeutic Nanoplatform with Infection and Inflammation Monitoring and Microenvironmental Regulation Accelerating Wound Repair. *ACS Appl. Mater. Interfaces* **2022**, *14* (34), 39172−39187.
(57) Wang, X.; Zhang, J.; Wang, Y.; Wang, C.; Xiao, J.; Zhang, Q.; Cheng, Y. Multi-Responsive Photothermal-Chemotherapy with Drug-Loaded Melanin-Like Nanoparticles for Synergetic Tumor Ablation. *Biomaterials* **2016**, *81*, 114−124.
(58) Yuan, Z.; Lin, C.; He, Y.; Tao, B.; Chen, M.; Zhang, J.; Liu, P.; Cai, K. Near-Infrared Light-Triggered Nitric-Oxide-Enhanced Photodynamic Therapy and Low-Temperature Photothermal Therapy for Biofilm Elimination. *ACS Nano* **2020**, *14* (3), 3546−3562.
(59) Peng, D.; Liu, G.; He, Y.; Gao, P.; Gou, S.; Wu, J.; Yu, J.; Liu, P.; Cai, K. Fabrication of a pH-Responsive Core−Shell Nanosystem with a Low-Temperature Photothermal Therapy Effect for Treating Bacterial Biofilm Infection. *Biomaterials Science* **2021**, *9* (22), 7483−7491.
(60) Yu, S.; Li, G.; Liu, R.; Ma, D.; Xue, W. Dendritic Fe_3O_4@ Poly (dopamine)@ PAMAM Nanocomposite as Controllable NO-Releasing Material: a Synergistic Photothermal and NO Antibacterial Study. *Adv. Funct. Mater.* **2018**, *28* (20), 1707440.
(61) Vaughn, A. R.; Haas, K. N.; Burney, W.; Andersen, E.; Clark, A. K.; Crawford, R.; Sivamani, R. K. Potential Role of Curcumin Against Biofilm-Producing Organisms on the Skin: A Review. *Phytotherapy Research* **2017**, *31* (12), 1807−1816.
(62) Shakeri, A.; Panahi, Y.; Johnston, T. P.; Sahebkar, A. Biological Properties of Metal Complexes of Curcumin. *BioFactors* **2019**, *45* (3), 304−317.
(63) Zhang, Y.-M.; Rock, C. O. Membrane Lipid Homeostasis in Bacteria. *Nature Reviews Microbiology* **2008**, *6* (3), 222−233.
(64) Xin, Q.; Shah, H.; Nawaz, A.; Xie, W.; Akram, M. Z.; Batool, A.; Tian, L.; Jan, S. U.; Boddula, R.; Guo, B.; Liu, Q.; Gong, J. R.

Antibacterial Carbon-Based Nanomaterials. *Adv. Mater.* **2019**, *31* (45), 1804838.
(65) Allobawi, R.; Ghelani, D. P.; Schneider-Futschik, E. K. Metabolomic Description of Ivacaftor Elevating Polymyxin B Mediated Antibacterial Activity in Cystic Fibrosis Pseudomonas Aeruginosa. *ACS Pharmacology & Translational Science* **2020**, *3* (3), 433−443.
(66) Qiang, L.; Jin, H.; Feng, Y.; Wu, R.; Song, Y.; Liu, L. Apoptosis-Like Bacterial Death Modulated by Photoactive Hyperthermia Nanomaterials and Enhanced Wound Disinfection Application. *Nanoscale* **2021**, *13* (35), 14785−14794.
(67) Lin, X.; Fang, Y.; Hao, Z.; Wu, H.; Zhao, M.; Wang, S.; Liu, Y. Bacteria-Triggered Multifunctional Hydrogel for Localized Chemodynamic and Low-Temperature Photothermal Sterilization. *Small* **2021**, *17* (51), 2103303.
(68) Wang, T.; Chen, X.; Luan, C.; Wu, J. High Throughput Lipid Profiling for Subtype Classification of Hepatocellular Carcinoma Cell Lines and Tumor Tissues. *Anal. Chim. Acta* **2020**, *1107*, 92−100.
(69) Chen, X.; Gao, J.; Wang, T.; Jiang, X.; Chen, J.; Liang, X.; Wu, J. Hepatocarcinoma Discrimination by Ratiometric Lipid Profiles Using Tip-Contact Sampling/Ionization Mass Spectrometry. *Analytical chemistry* **2019**, *91* (16), 10376−10380.
(70) Chen, X.; Wang, T.; Lin, L.; Wo, F.; Liu, Y.; Liang, X.; Ye, H.; Wu, J. Tip-Enhanced Photoinduced Electron Transfer and Ionization on Vertical Silicon Nanowires. *ACS Appl. Mater. Interfaces* **2018**, *10* (17), 14389−14398.
(71) Liu, X.; Chen, Z.; Wang, T.; Jiang, X.; Qu, X.; Duan, W.; Xi, F.; He, Z.; Wu, J. Tissue Imprinting on 2D Nanoflakes-Capped Silicon Nanowires for Lipidomic Mass Spectrometry Imaging and Cancer Diagnosis. *ACS Nano* **2022**, *16* (4), 6916−6928.
(72) Lopalco, P.; Lobasso, S.; Lopes-dos-Santos, R. M. A.; Van Stappen, G.; Corcelli, A. Lipid Profile Changes During the Development of Artemia franciscana, From Cysts to the First Two Naupliar Stages. *Frontiers in Physiology* **2019**, *9*, 1872.
(73) Matsumoto, K.; Kusaka, J.; Nishibori, A.; Hara, H. Lipid Domains in Bacterial Membranes. *Mol. Microbiol.* **2006**, *61* (5), 1110−1117.
(74) Qian, S.; Wang, J.; Liu, Z.; Mao, J.; Zhao, B.; Mao, X.; Zhang, L.; Cheng, L.; Zhang, Y.; Sun, X.; Cui, W. Secretory Fluid-Aggregated Janus Electrospun Short Fiber Scaffold for Wound Healing. *Small* **2022**, *18*, 2200799.
(75) Mahmood, S.; Bhattarai, P.; Khan, N. R.; Subhan, Z.; Razaque, G.; Albarqi, H. A.; Alqahtani, A. A.; Alasiri, A.; Zhu, L. An Investigation for Skin Tissue Regeneration Enhancement/Augmentation by Curcumin-Loaded Self-Emulsifying Drug Delivery System (SEDDS). *Polymers* **2022**, *14* (14), 2904.
(76) Mirzahosseinipour, M.; Khorsandi, K.; Hosseinzadeh, R.; Ghazaeian, M.; Shahidi, F. K. Antimicrobial Photodynamic and Wound Healing Activity of Curcumin Encapsulated in Silica Nanoparticles. *Photodiagnosis and Photodynamic Therapy* **2020**, *29*, 101639.
(77) Zhang, X.; Min, Y.; Zhang, Q.; Wu, S.; Fu, W.; Wu, J.; Li, M.; Wang, Y.; Zhang, P. Functionalized Mn_3O_4 Nanosheets with Photothermal, Photodynamic, and Oxidase-Like Activities Triggered by Low-Powered Near-Infrared Light for Synergetic Combating Multidrug-Resistant Bacterial Infections. *Adv. Healthcare Mater.* **2022**, *11* (12), 2200121.

https://doi.org/10.1021/acsami.2c12012
ACS Appl. Mater. Interfaces 2022, 14, 48368−48383